THE ASTROPHYSICAL JOURNAL, 418:368–385, 1993 November 20

VLA OBSERVATIONS OF STRONG *IRAS* POINT SOURCES ASSOCIATED WITH COMPACT H II REGIONS

GUIDO GARAY,[1] LUIS F. RODRÍGUEZ,[2] JAMES M. MORAN,[3] AND ED CHURCHWELL[4]
Received 1992 November 6; accepted 1993 April 27

ABSTRACT

We present multifrequency radio continuum observations made with the Very Large Array of a sample of 16 strong *IRAS* point sources associated with compact H II regions. Twelve sources were observed at 1.5, 4.9, and 15.0 GHz, with angular resolution of ~15″, 5″, and 3″, respectively. Three were observed at 1.5 and 4.9 GHz, and one at 1.5 GHz. The radio continuum brightness distribution was resolved for all sources. Nine objects show simple morphologies: core-halo (2), shell (3), cometary (3), and bipolar (1), consistent with their being excited by a single star. The remaining seven sources show complex radio structure. The average infrared luminosity of the complex sources is 3 times larger than that of the simple sources. The morphologies of the complex H II regions, which can be decomposed into multiple components, together with their large IR luminosities, suggest that these regions are excited by a cluster of stars. Furthermore, the observed infrared and radio properties suggest that the cluster contains only massive stars (O and early B spectral types).

About 70% of the individual regions of ionized gas have linear diameters between 0.1 and 1 pc and electron densities between 10^3 and 10^4 cm^{-3}, corresponding to H II regions of class II in the classification scheme of Habing & Israel (1979). The electron densities and diameters follow a power-law relation of the form $N_e \propto D^{-1}$. For the sources showing simple morphologies, the ratio between the total infrared and Lyman-α luminosities ranges from 6 to 21. If single stars excite these *simple* H II regions, then the infrared excesses are fully accounted for by dust emission in large, cool envelopes heated by stellar photons longward of the Lyman continuum limit and by optical/near-infrared photons emitted by hot dust within the H II regions. The fraction of Lyman continuum photons absorbed by dust within the H II regions is typically 55%.

Subject headings: H II regions — interstellar: continuum — radio continuum: interstellar

1. INTRODUCTION

Newly formed massive stars embedded in molecular clouds are intimately associated with compact regions of ionized gas and compact regions of warm dust and molecular gas. Since O and B stars emit the bulk of their radiation at wavelengths shorter than the Lyman continuum limit, they ionize the dense molecular gas and heat the dust grains around them, producing compact H II regions. In addition, circumstellar dust surrounding the region of ionized gas absorbs all the stellar radiation, either directly or after being processed in the nebula, producing compact regions of warm dust that reemit the absorbed energy in the far-infrared (FIR). Compact H II regions are thus invariably associated with strong IR sources.

Estimates of the amount of dust within the ionized gas region remains uncertain. Wood & Churchwell (1989) suggested that the fraction of UV photons absorbed by dust within compact H II regions could be as high as 90%. On the other hand, Chini, Krugel, & Wargau (1987) and Churchwell, Wolfire, & Wood (1990b) concluded that the exciting stars of compact H II regions are surrounded by a dust cocoon with a large, evacuated central cavity. More observational data, particularly at radio and infrared wavelengths with similar angular resolutions, are needed to clarify this issue.

We report here radio observations, made with the Very Large Array with angular resolutions of 15″, 5″, and 3″, toward 14 fields containing *IRAS* point sources. The lower resolution observations were designed to allow a meaningful comparison of the global radio and infrared properties, in particular to determine the role of dust within the H II region. The higher resolution observations were designed to study the extent and morphology of the ionized gas, in particular to determine whether the *IRAS* point sources are excited by single stars rather than clusters of stars. The objects were selected from the lists of strong *IRAS* sources associated with compact H II regions observed at 1.3 mm wavelength by Chini et al. (1986a, b).

2. OBSERVATIONS

The observations were made at the Very Large Array (VLA) of the National Radio Astronomy Observatory,[5] during 1988 March 27. The array was in a C/D hybrid configuration with baselines ranging from 0.5 to 3.4 km. The instrumental parameters are given in Table 1.

We observed 14 fields, centered near *IRAS* point sources associated with compact H II regions, at the frequencies of 1.465, 4.885, and 14.965 GHz, using an effective bandwidth of 100 MHz and 26 antennas. The observations were conducted in the snapshot mode. At 1.5 and 4.9 GHz, the integration times on-source were ~5.5 minutes, while at 15.0 GHz they were ~8.2 minutes. Calibration sources were observed for ~3 minutes, at intervals of 12 minutes, at 1.5 and 4.9 GHz, and for

[1] Departamento de Astronomía, Universidad de Chile, Casilla 36-D, Santiago, Chile.
[2] Instituto de Astronomía, UNAM, Apartado Postal 70-264, 04510 México, D.F., México.
[3] Harvard-Smithsonian Center for Astrophysics, 60 Garden Street, Cambridge, MA 02138.
[4] Washburn Observatory, University of Wisconsin–Madison, 475 North Charter Street, Madison, WI 53706.

[5] The National Radio Astronomy Observatory is operated by Associated Universities, Inc., under cooperative agreement with the National Science Foundation.

~3 minutes, at intervals of 9 minutes, at 15.0 GHz, in order to correct the amplitude and phase of the interferometer data for atmospheric and instrumental effects. The flux density level was referred to 3C 286, which was assumed to have flux densities of 14.4, 7.43, and 3.45 Jy at 1.5, 4.9, and 15.0 GHz, respectively. The data were edited and calibrated using the standard VLA programs. Maps of the whole primary field of view were produced by Fourier transformation of the (u, v) data. The resulting synthesized beams are given in columns (7)–(9) of Table 1.

3. RESULTS

Maps of the radio continuum emission from the 16 *IRAS* point sources are shown in Figures 1–16. The smoother appearance of the 1.5 GHz maps is due to the lower angular resolution and the moderately high opacity of the radio continuum emission at that frequency. At higher frequencies (i.e., higher angular resolutions) the structure of the radio sources is clearly resolved, demonstrating that these observations are better suited for studying structural details. The *IRAS* positions, indicated in the 1.5 GHz maps as crosses, are in good agreement with the radio positions. In only one case, source G10.5+0.0, is the *IRAS* position considerably displaced from the radio continuum position. The average displacement between the peak radio and *IRAS* positions, for the sources exhibiting simple morphologies, is 8″ ± 7″.

The radio brightness distributions of nine out of 16 sources are consistent with excitation by a single star. The positions, flux densities, and angular sizes of these sources are given in Table 2. Their morphological types, following the classification scheme suggested by Wood & Churchwell (1989), are core-halo (two sources), shell (three sources), cometary (three sources),

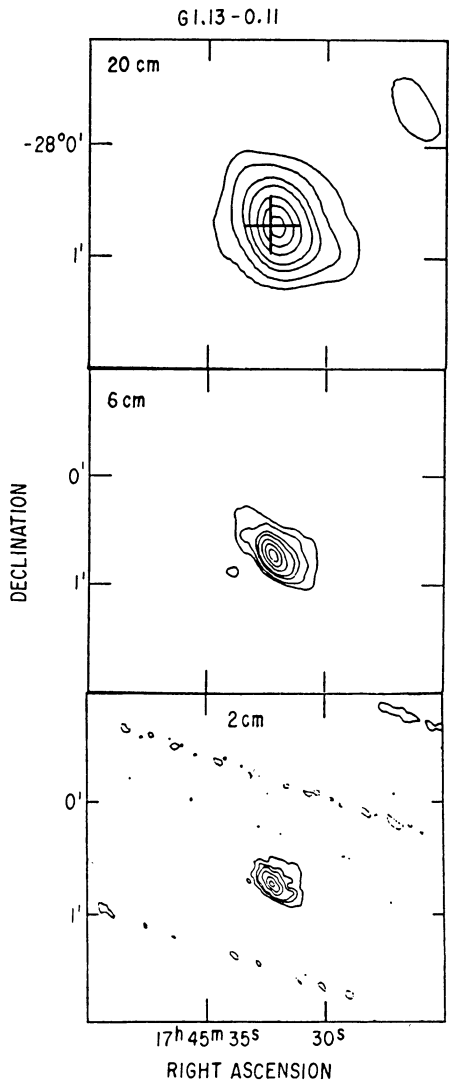

FIG. 1.—VLA radio continuum maps of G1.13−0.11. *Upper panel:* 1.5 GHz map with 19″ resolution. Contour levels are −5, 5, 10, 20, 30, 50, 70, and 90% of the peak flux density of 0.821 Jy beam^{-1}. *Middle panel:* 4.9 GHz map with 5″ resolution. Contour levels are −5, 5, 10, 20, 30, 50, 70, and 90% of the peak flux density of 0.210 Jy beam^{-1}. *Lower panel:* 15 GHz map with 3″ resolution. Contour levels are −10, 10, 20, 30, 50, 70, and 90% of the peak flux density of 0.084 Jy beam^{-1}.

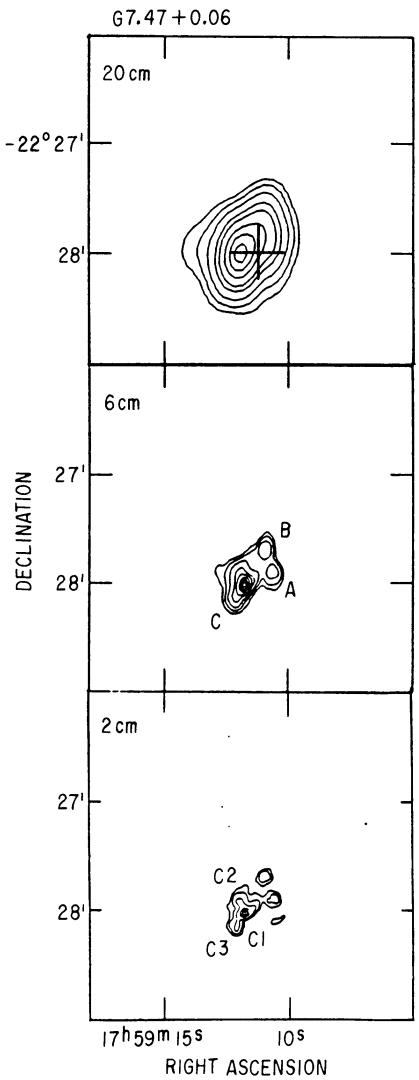

FIG. 2.—VLA radio continuum maps of G7.47+0.06. *Upper panel:* 1.5 GHz map with 17″ resolution. Contour levels are −2.5, 2.5, 5, 10, 20, 30, 50, 70, and 90% of the peak flux density of 0.723 Jy beam^{-1}. *Middle panel:* 4.9 GHz map with 5″ resolution. Contour levels are −2.5, 2.5, 5, 10, 20, 30, 50, 70, and 90% of the peak flux density of 0.374 Jy beam^{-1}. *Lower panel:* 15 GHz map with 3″ resolution. Contour levels are −2.5, 2.5, 5, 10, 30, 50, 70, and 90% of the peak flux density of 0.289 Jy beam^{-1}.

TABLE 1

INSTRUMENTAL PARAMETERS

Source (1)	Phase Tracking Center α(1950) (2)	Phase Tracking Center δ(1950) (3)	Integration Time (minutes) 1.5 GHz (4)	Integration Time (minutes) 4.9 GHz (5)	Integration Time (minutes) 15 GHz (6)	Synthesized Beam 1.5 GHz (7)	Synthesized Beam 4.9 GHz (8)	Synthesized Beam 15 GHz (9)
G1.13−0.11	$17^h45^m31^s.7$	−28°00′44″	5.7	5.0	8.0	26.4 × 13.2	8.3 × 3.4	3.2 × 2.6
G7.47+0.06	17 59 11.3	−22 28 01	5.7	5.7	8.3	22.8 × 13.2	7.0 × 3.4	3.0 × 2.5
G9.61+0.20	18 03 14.5	−20 32 11	5.3	5.3	8.7	20.1 × 12.2	6.6 × 3.5	3.0 × 2.6
G10.5+0.0	18 05 40.4	−19 52 20	5.7	5.9	8.3	19.6 × 12.4	6.6 × 3.4	2.7 × 2.2
G13.87+0.28	18 11 41.7	−16 46 35	5.6	5.7	8.3	19.1 × 12.5	6.0 × 3.5	2.9 × 2.6
G24.47+0.49	18 31 26.4	−07 20 32	5.3	4.9	8.3	14.6 × 12.8	4.5 × 3.9	2.8 × 2.7
G23.87−0.12	18 32 30.2	−08 09 20	6.0	5.6	8.2	14.4 × 12.9	4.6 × 3.8	2.9 × 2.7
G25.4−0.2	18 35 31.1	−06 51 20	5.7	5.3	...	14.7 × 13.2	4.6 × 3.9	...
G31.41+0.31	18 44 59.0	−01 16 07	5.4	5.7	8.1	14.3 × 13.6	4.4 × 4.0	2.9 × 2.5
G32.80+0.19	18 47 56.7	−00 05 31	4.7	5.3	8.3	14.1 × 13.8	4.2 × 4.0	2.5 × 2.3
G33.91+0.11	18 50 17.3	00 51 45	5.5	6.0	7.8	13.5 × 13.2	4.3 × 4.1	2.9 × 2.6
G45.5+0.1	19 11 47.3	11 07 02	5.3	5.3	8.3	17.6 × 15.8	5.1 × 4.4	2.7 × 2.6
G61.47+0.09	19 44 41.3	25 05 04	5.3	5.3	...	14.9 × 13.5	4.4 × 3.8	...
G75.8+0.4	20 19 47.3	37 21 36	5.7	5.7	8.3	15.5 × 12.8	4.7 × 3.7	2.7 × 2.7

and bipolar (one source). For the remaining sources, two or more radio components are detected, suggesting that the ionized gas is excited by a cluster of young O and B stars. Table 3 lists the observed parameters of the complex H II regions.

We have calculated physical parameters of the ionized gas, following the formulation of Mezger & Henderson (1967), on the assumption that the H II regions have constant electron density and an electron temperature of 10^4 K. For all except the shell sources, we assumed that the volume V is given by $(\pi/6)(1.471)^3(\theta_g D)^3$, where θ_g is the geometrical mean angular diameter at half-maximum and D the distance to the source (see Panagia & Walmsley 1978 for an additional correction on the estimate of the source angular radius from the observed

TABLE 2

OBSERVED PARAMETERS OF SIMPLE H II REGIONS

Source (1)	*IRAS* Identification (2)	α(1950)[a] (3)	δ(1950)[a] (4)	Frequency (GHz) (5)	Flux Density[b] (Jy) (6)	Angular Size (arcsec) (7)	Morphology (8)
G1.13−0.11	17455−2800	$17^h45^m32^s.2$	−28°00′44″	1.5	2.37 ± 0.05	22	Core-halo
				4.9	1.93 ± 0.01	14	
				15.0	1.47 ± 0.01	13	
G13.87+0.28	18116−1646	18 11 41.7	−16 46 37	1.5	3.47 ± 0.07	24	Cometary
				4.9	3.86 ± 0.02	20	
				15.0	2.39 ± 0.01	19	
G24.47+0.49	18314−0720	18 31 26.7	−07 20 24	1.5	4.17 ± 0.02	46/33[c]	Shell
				4.9	3.51 ± 0.03	...	
				15.0	0.88 ± 0.02	[d]	
G23.87−0.12	18324−0809						
A	...	18 32 30.9	−08 09 18	1.5	0.81 ± 0.02	39/25[c]	Shell/cometary
				4.9	1.05 ± 0.02	...	
B	...	18 32 30.7	−08 09 50	1.5	0.040 ± 0.008	8	Spherical
				4.9	0.049 ± 0.002	4	
				15.0	0.046 ± 0.001	4	
G31.41+0.31	18449−0115	18 44 59.2	−01 16 08	1.5	0.96 ± 0.03	10	Cometary
				4.9	1.06 ± 0.02	8	
				15.0	0.77 ± 0.01	8	
G33.91+0.11	18502+0051	18 50 17.5	00 51 46	1.5	0.80 ± 0.04	11	Core-halo
				4.9	1.09 ± 0.03	6	
				15.0	0.73 ± 0.02	4	
G45.48+0.13	19117+1107	19 11 46.4	11 07 28(A)	1.5	1.55 ± 0.03	11/16[e]	Bipolar
		19 11 47.3	11 07 12(B)	4.9	1.33 ± 0.02	16/17[e]	
				15.0	1.19 ± 0.02	12/18[e]	
G75.77+0.34	20198+3716	20 19 49.7	37 16 15	1.5	4.73 ± 0.03	36	Cometary
G75.84+0.40	20197+3721	20 19 47.3	37 21 33	1.5	7.09 ± 0.08	27	Shell
				4.9	8.56 ± 0.02	28	
				15.0	4.40 ± 0.03	[d]	

[a] Positions are accurate to ±1″ (3 σ).

[b] Quoted errors are formal 1 σ errors arising from the integration of the flux/beam over a rectangular box enclosing the source; due to calibration uncertainties, flux densities are, however, probably accurate to ±5%.

[c] Outer/inner radius of shell.

[d] Partially resolved.

[e] Size of lobe A/B.

TABLE 3

OBSERVED PARAMETERS OF COMPLEX H II REGIONS

Source (Component) (1)	α(1950) (2)	δ(1950) (3)	Frequency (GHz) (4)	Flux Density (Jy) (5)	Angular Size (arcsec) (6)	Morphology (7)
G7.47+0.06 (17591−2228):[a]						
A + B	...	...	1.5	0.42 ± 0.02	12	
A	17h59m10s.6	−22°27′53″	4.9	0.18 ± 0.01	9	Spherical
			15.0	0.13 ± 0.002	8	
B	17 59 11.0	−22 27 41	4.9	0.20 ± 0.01	8	Spherical
			15.0	0.15 ± 0.002	6	
C1 + C2 + C3	...	...	1.5	1.19 ± 0.02	14	
			4.9	1.31 ± 0.04	8	
C1	17 59 11.8	−22 28 02	15.0	0.53 ± 0.01	3	Spherical
C2	17 59 12.0	−22 27 55	15.0	0.44 ± 0.01	9	Spherical
C3	17 59 12.2	−22 28 09	15.0	0.39 ± 0.01	9	Spherical
G9.61+0.20 (18032−2032):						
A	18 03 13.1	−20 32 02	1.5	0.40 ± 0.01	32	Shell?
			4.9	0.27 ± 0.01	...	
			15.0	[b]	...	
B + C + D + E	...	...	1.5	0.68 ± 0.01	15	
B	18 03 15.3	−20 32 04	4.9	0.64 ± 0.01	15	Cometary
			15.0	0.56 ± 0.01	14	
C	18 03 15.6	−20 31 46	4.9	0.050 ± 0.002	3	Spherical
			15.0	0.024 ± 0.002	2	
D	18 03 16.1	−20 32 04	4.9	0.070 ± 0.009	2	Spherical
			15.0	0.11 ± 0.006	1	
E	18 03 15.9	−20 31 53	15.0	0.019 ± 0.002	2	Spherical
G10.46+0.03 (18056−1952):						
A	18 05 38.6	−19 52 46	4.9	0.034 ± 0.002	6	Spherical
			15.0	0.013 ± 0.001	2	
B	18 05 37.5	−19 52 40	1.5	0.33 ± 0.01	9	Cometary
			4.9	0.38 ± 0.01	7	
			15.0	0.16 ± 0.002	3	
C	18 05 38.1	−19 53 03	1.5	0.39 ± 0.01	45	Irregular
			4.9	[b]	...	
			15.0	[b]	...	
G10.44+0.01	18 05 39.8	−19 54 29	1.5	0.22 ± 0.01	30[c]	Core-halo
			4.9	0.15 ± 0.01	18[d]	
G10.47+0.03	18 05 40.4	−19 52 17	1.5	0.19 ± 0.01	~23	Irregular
AB	18 05 40.3	−19 52 21	4.9	0.043 ± 0.001	<2	Spherical
			15.0	0.142 ± 0.003	1	
C	18 05 40.4	−19 52 17	1.5	0.033 ± 0.002	...	
			4.9	0.036 ± 0.001	3	Spherical
			15.0	0.020 ± 0.001	<1	
G25.40−0.14	18 35 26.8	−06 48 38	1.5	2.48 ± 0.08	14	Core-halo
			4.9	4.44 ± 0.04	9	
G25.38−0.18 (18355−0650):						
Whole	18 35 33.6	−06 50 34	1.5	10.6	~90	Irregular
Core	...	...	1.5	4.79 ± 0.07	33	Bipolar?
			4.9	3.19 ± 0.04	...	
G32.80+0.19 (18479−0005):						
A + B	...	...	1.5	1.49 ± 0.02	11	
A	18 47 56.8	−00 05 34	4.9	0.90 ± 0.05	2	Spherical
			15.0	1.15 ± 0.04	2	
B	18 47 57.1	−00 05 29	4.9	2.25 ± 0.05	8	Cometary
			15.0	1.21 ± 0.03	[b]	
G45.45+0.06 (19120+1103)	19 12 00.0	11 03 58	1.5	3.81 ± 0.07	28	Core-halo
			4.9	4.02 ± 0.04	10	
G61.47+0.09 (19446+2505):						
B1 + B2	...	...	1.5	4.51 ± 0.08	21	
B1	19 44 42.7	25 05 21	4.9	4.36 ± 0.02	17	Cometary
B2	19 44 43.4	25 05 20	4.9	0.83 ± 0.05	6	Spherical

[a] *IRAS* identification in parentheses.
[b] Partially resolved.
[c] Halo size.
[d] Core size.

Gaussian angular size). For the shell sources we assumed $V = (\pi/6)(\theta_o^3 - \theta_i^3)D^3$, where θ_o and θ_i are the outer and inner diameters of the shell, respectively. For the derivation of physical parameters we used, wherever possible, the distances given by Churchwell, Walmsley, & Cesaroni (1990a) that correspond to the kinematic distances determined using a rotation curve with an orbital velocity of 220 km s^{-1} at 8.5 kpc from the Galactic center (Brand 1986). Table 4 lists the distance (col. [2]), the observing frequency used in the calculations (col. [3]), and the derived parameters: diameter (col. [4]), electron density (col. [5]), emission measure (col. [6]), continuum optical depth (col. [7]), number of ionizing photons required to maintain the ionization of the nebula (col. [8]), and spectral type (col. [9]).

4. COMMENTS ON INDIVIDUAL SOURCES

4.1. *G1.13−0.11*

G1.13−0.11 is presumably in the Galactic center region, hence at a distance of 8.5 kpc from the Sun. It is embedded in,

TABLE 4

PHYSICAL PARAMETERS

Source (1)	D (kpc) (2)	Frequency (GHz) (3)	Diameter (pc) (4)	N_e (cm^{-3}) (5)	EM (pc cm^{-6}) (6)	τ (7)	N_c' (10^{49} s^{-1}) (8)	Spectral Type (9)
A. Simple Sources								
G1.13−0.11	8.5							
Halo	...	1.5	0.91	1.2×10^3	1.9×10^6	0.27	1.35	O6
Core	...	15.0	0.55	2.3×10^3	4.1×10^6	0.004	1.06	...
G13.87+0.28	4.4	4.9	0.43	2.5×10^3	4.1×10^6	0.047	0.66	O6.5
G24.47+0.49	9.4	1.5	1.50/2.09[a]	1.1×10^3	2.7×10^6	0.11	2.91	O5.5
G23.87−0.12	10.6							
A	...	1.5	1.28/2.00[a]	5.5×10^2	6.8×10^5	0.064	1.05	O6
B	...	4.9	0.18	2.6×10^3	1.8×10^6	0.021	0.049	O9.5
G31.41+0.31	7.9	4.9	0.32	3.7×10^3	6.6×10^6	0.077	0.59	O6.5
G33.91+0.11	8.3							
Halo	...	1.5	0.43	2.1×10^3	2.8×10^6	0.41	...	...
		4.9	0.25	5.9×10^3	1.3×10^7	0.15	0.67	O6.5
Core	...	15.0	0.16	9.7×10^3	2.2×10^7	0.024	...	...
G45.48+0.13	6.0							
A	...	1.5	0.33	1.8×10^3	1.5×10^6	0.22	0.14	O8.5
B	...	1.5	0.46	1.5×10^3	1.6×10^6	0.24	0.30	O7.5
G75.84+0.40	4.1	4.9	0.56/0.70[a]	4.5×10^3	1.2×10^7	0.055	1.28	O6
G75.77+0.34	4.1	1.5	0.71	1.1×10^3	1.3×10^6	0.19	0.58	O6.5
B. Complex Sources								
G7.47+0.06	6.3							
A	...	4.9	0.28	1.5×10^3	9.6×10^5	0.011	0.064	O9.5
B	...	4.9	0.25	1.9×10^3	1.3×10^6	0.015	0.071	O9.5
C1	...	15.0	0.080	1.8×10^4	3.8×10^7	0.041	0.21	O8
C2	...	15.0	0.27	2.6×10^3	2.7×10^6	0.003	0.17	O8.5
C3	...	15.0	0.27	2.5×10^3	2.4×10^6	0.003	0.15	O8.5
G9.61+0.20	16.1							
A	...	1.5	2.49	2.0×10^2	1.5×10^5	0.022	0.82	O6.5
B	...	4.9	1.14	8.9×10^2	1.3×10^6	0.015	1.48	O6
C	...	4.9	0.22	3.0×10^3	2.8×10^6	0.033	0.12	O9
D	...	4.9	0.17	5.3×10^3	6.8×10^6	0.079	0.16	O8.5
E	...	15.0	0.17	2.9×10^3	2.0×10^6	0.002	0.049	O9.5
G10.46+0.03	5.8							
A	...	4.9	0.19	3.6×10^3	3.7×10^6	0.043	0.11	O9
B	...	4.9	0.17	1.2×10^3	3.9×10^5	0.004	0.010	B0
C	...	1.5	1.27	2.0×10^2	7.4×10^4	0.011	0.10	O9
G10.44+0.01	5.8	1.5	0.83	2.8×10^2	9.6×10^4	0.014	0.058	O9.5
G10.47+0.03	5.8							
AB	...	15.0	0.019	7.5×10^4	1.5×10^8	0.17	0.048	O9.5
C	...	4.9	0.076	4.4×10^3	2.2×10^6	0.025	0.011	B0
G25.40−0.14	9.6	4.9	0.42	6.2×10^3	2.4×10^7	0.28	3.64	O5
G25.38−0.18	10.8							
Whole	...	1.5	4.71	2.7×10^2	5.1×10^5	0.074	9.75	O4
Core	...	1.5	1.72	8.2×10^2	1.7×10^6	0.25	4.41	O5
G32.80+0.19	13.0							
A	...	15.0	0.11	3.5×10^4	2.0×10^8	0.21	1.93	O5.5
B	...	4.9	0.48	4.8×10^3	1.6×10^7	0.19	3.21	O5
G45.45+0.06	6.6							
Halo	...	1.5	0.91	1.2×10^3	1.8×10^6	0.27	1.31	O6
Core	...	4.9	0.32	6.0×10^3	1.7×10^7	0.20	1.56	O6
G61.47+0.09	5.4							
B1	...	4.9	0.44	3.2×10^3	6.7×10^6	0.078	1.13	O6
B2	...	4.9	0.16	6.4×10^3	9.6×10^6	0.11	0.22	O8

[a] Inner/outer diameter of the shell.

or projected toward, a giant region of ionized gas of ~12 pc in size (Downes et al. 1979). Our VLA observations show that G1.13−0.11 is an optically thin H II region that has a core-halo structure, with a halo of ~1.2 × 0.7 pc in diameter and a core of ~0.8 × 0.4 pc. The core was previously mapped at 5 GHz, with the Westerbork Synthesis Radio Telescope (WSRT), by Downes et al. (1979).

4.2. *G7.47+0.06*

G7.47+0.06 was interferometrically mapped at 2.7 and 8.1 GHz by Wink, Altenhoff, & Mezger (1982, hereafter WAM). The distance to this source is uncertain. We adopt the value of 6.3 kpc suggested by WAM, derived assuming that this H II region belongs to the "3 kpc" arm. Our VLA map at 5 GHz (see Fig. 2) shows that G7.47+0.06 consists of a main bright component (labeled C) and two weaker components west of the main source (labeled A and B), suggesting that this region is being excited by a cluster of young O and B stars rather than by a single star. The main source itself shows complex structure, which we model as a bright and compact (0.08 pc in diameter) component (C1) near its center and two weaker and more extended (~0.3 pc in diameter each) components (C2 and C3) toward the northeast and southeast of the brighter components, respectively.

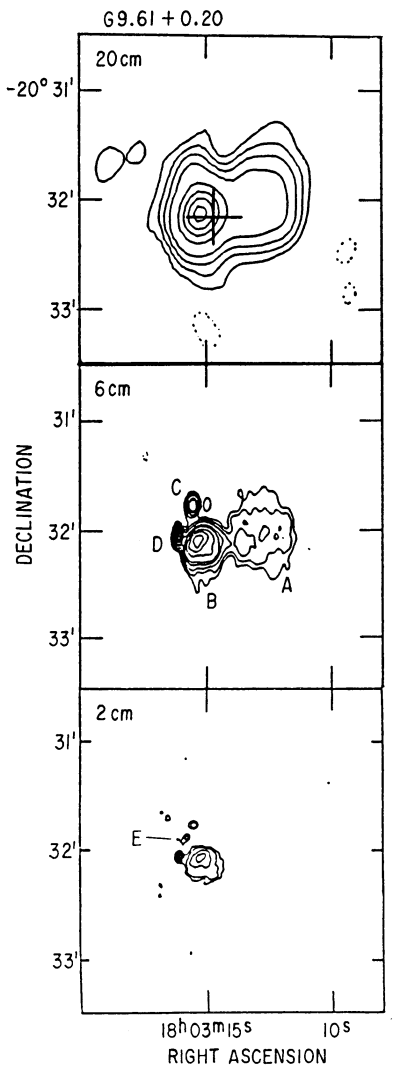

FIG. 3.—VLA radio continuum maps of G9.61+0.20. *Upper panel:* 1.5 GHz map with 16″ resolution. Contour levels are −1, 1, 2.5, 5, 10, 30, 50, 70, and 90% of the peak flux density of 0.371 Jy beam^{-1}. *Middle panel:* 4.9 GHz map with 5″ resolution. Contour levels are −2.5, 2.5, 5, 10, 20, 30, 50, 70, and 90% of the peak flux density of 0.073 Jy beam^{-1}. *Lower panel:* 15 GHz map with 3″ resolution. Contour levels are −5, 5, 10, 20, 30, 50, 70, and 90% of the peak flux density of 0.082 Jy beam^{-1}.

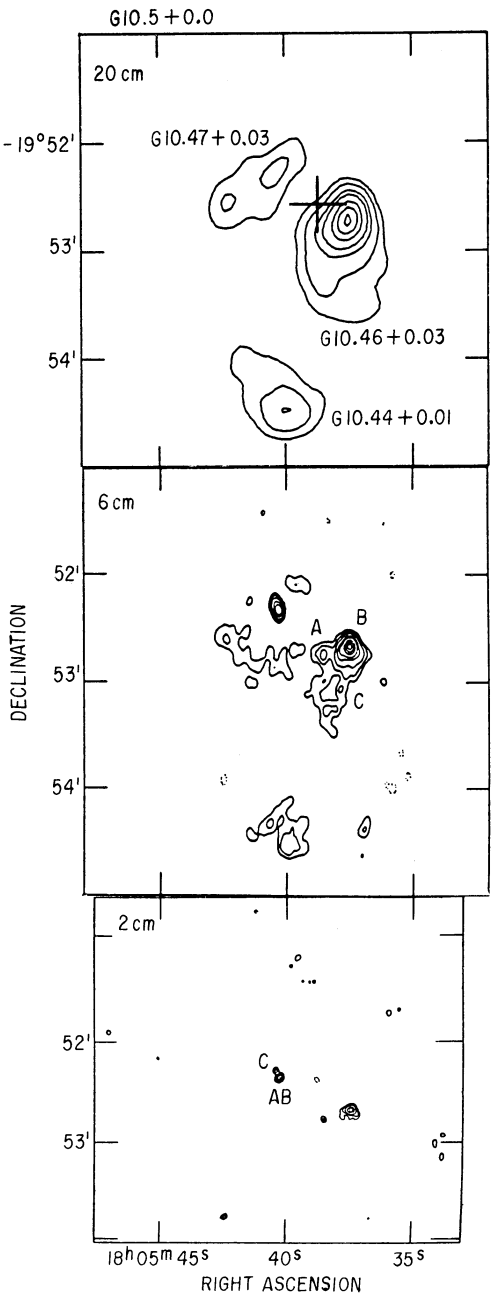

FIG. 4.—VLA radio continuum maps of G10.5+0.0. *Upper panel:* 1.5 GHz map with 16″ resolution. Contour levels are −5, 5, 10, 20, 30, 50, 70, and 90% of the peak flux density of 0.270 Jy beam^{-1}. *Middle panel:* 4.9 GHz map with 5″ resolution. Contour levels are −2.5, 2.5, 5, 10, 20, 30, 50, 70, and 90% of the peak flux density of 0.113 Jy beam^{-1}. *Lower panel:* 15 GHz map with 2″ resolution. Contour levels are −2.5, 2.5, 5, 10, 20, 30, 50, 70, and 90% of the peak flux density of 0.119 Jy beam^{-1}.

4.3. *G9.61+0.20*

This source was previously interferometrically mapped at 2.7 and 8.1 GHz by WAM. Our VLA maps (see Fig. 3) show it to be a complex region of ionized gas consisting of five objects: (1) a western, low brightness temperature (~180 K at 1.5 GHz) extended (~32″ in diameter) H II region, seen in the 1.5 and 4.9 GHz maps but resolved out in the 15 GHz map; (2) a central cometary-shaped object with an angular diameter of ~15″ and a peak brightness temperature of ~810 K at 1.5 GHz; and (3) three compact H II regions toward the northeast. From a comparison of the luminosities derived from radio and infrared observations we concluded that this source, whose distance ambiguity has not been previously resolved (cf. Downes et al. 1980), is likely to be at the far kinematic distance (see discussion in § 5.2).

4.4. *G10.5+0.0*

Our interferometric observations reveal several sources toward the $l = 10.^{\circ}5$, $b = 0.^{\circ}0$ Galactic direction. The 1.5 GHz map (see Fig. 4) shows that there are three complexes spread over a region of ~3′ in diameter: (1) an easterly component, G10.46+0.03, with a total flux density of 0.67 Jy; (2) a northern elongated component, G10.47+0.03, with a flux density of 0.19 Jy and angular diameters of ~32″ × 16″; and (3) a southern component, G10.44+0.01, with a flux density of 0.22 Jy and a size of ~30″. The total flux density contained in our 1.5 GHz map (16″ angular resolution) is 1.09 Jy, corresponding to ~80% of that measured with single-dish telescopes (1.35 Jy at 4.9 GHz [WAM]; 1.37 Jy at 10 GHz [Handa et al. 1987]).

The northern complex, G10.47+0.03, appears considerably different in the 4.9 and 15 GHz maps than in the 1.5 GHz map. At the higher frequencies the low-brightness extended emission seen at 1.5 GHz is almost completely resolved, while a compact

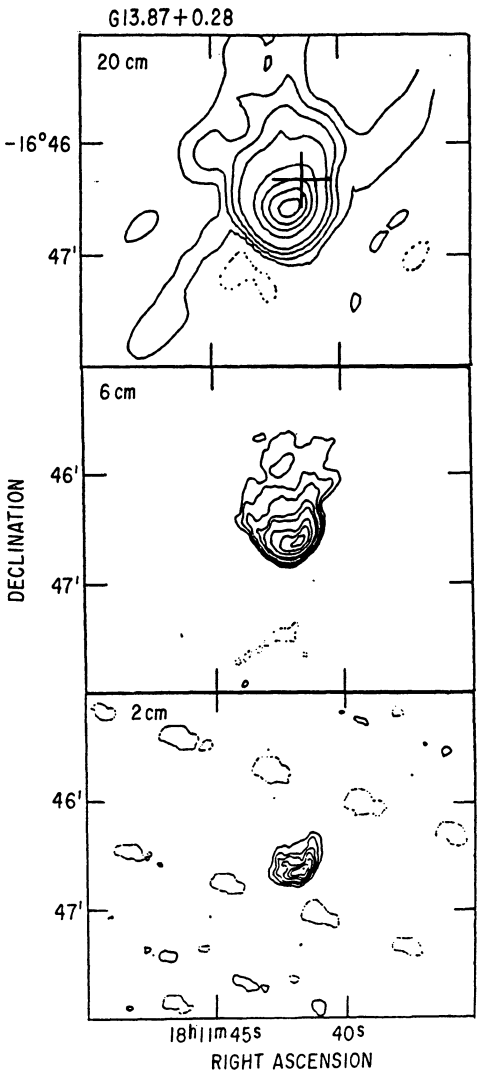

FIG. 5.—VLA radio continuum maps of G13.87+0.28. *Upper panel:* 1.5 GHz map with 15″ resolution. Contour levels are −1, 1, 2.5, 5, 10, 30, 50, 70, and 90% of the peak flux density of 0.956 Jy beam^{-1}. *Middle panel:* 4.9 GHz map with 5″ resolution. Contour levels are −2.5, 2.5, 5, 10, 20, 30, 50, 70, and 90% of the peak flux density of 0.187 Jy beam^{-1}. *Lower panel:* 15 GHz map with 3″ resolution. Contour levels are −10, 10, 20, 30, 40, 50, 60, and 70 mJy beam^{-1}.

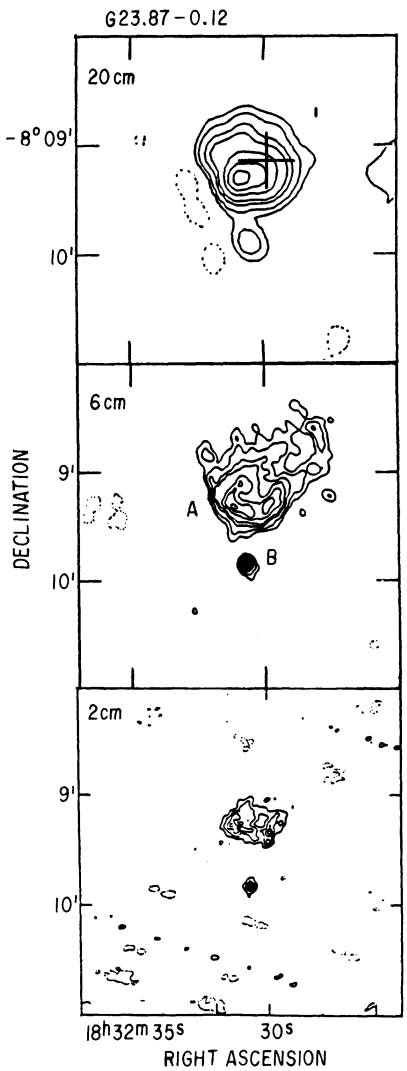

FIG. 6.—VLA radio continuum maps of G23.87−0.12. *Upper panel:* 1.5 GHz map with 14″ resolution. Contour levels are −5, 5, 10, 20, 30, 50, 70, and 90% of the peak flux density of 0.186 Jy beam^{-1}. *Middle panel:* 4.9 GHz map with 4″ resolution. Contour levels are −5, 5, 10, 20, 30, 50, 70, and 90% of the peak flux density of 0.028 Jy beam^{-1}. *Lower panel:* 15 GHz map with 3″ resolution. Contour levels are −1, 1, 2, 3, 4, 5, 6, and 7 times 2.5 mJy beam^{-1}.

double source is visible. Higher angular resolution observations by Wood & Churchwell (1989) showed that the brightest component at 15 GHz (AB in Fig. 4) actually consists of two ultracompact components.

The observations of 4.9 and 15 GHz show that the G10.46+0.03 complex consists of three components: (1) a bright, cometary-shaped region (labeled B); (2) an extended, low brightness temperature region toward the south (labeled C); and (3) a compact source toward the east (labeled A). Components A and B were previously detected at 4.9 GHz by Wood & Churchwell (1989).

4.5. *G13.87+0.28*

Our VLA observations show that G13.87+0.28 has a cometary morphology, exhibiting a head with a sharp edge toward the southwest and a long tail trailing to the northeast. The total flux density contained in our 1.5 GHz map, of 3.47 Jy, is in good agreement with the flux density at 2.7 GHz, of 3.61 Jy, measured by WAM.

4.6. *G23.87−0.12*

This source was previously mapped at 2.7 and 8.1 GHz by WAM. Our VLA observations show that G23.87−0.12 consists of two regions of ionized gas: (1) a northern extended component exhibiting a partial shell structure with an outer radius of ~1.0 pc, suggesting that it is an evolved H II region; and (2) a southern compact component with a diameter of ~0.2 pc.

4.7. *G24.47+0.49*

Our VLA observations at 1.5 and 5 GHz show that this H II region has a shell structure, with inner and outer angular diameters of ~33″ and 46″, respectively. At 15 GHz our VLA map contains ~20% of the total flux (4.17 Jy) measured at 1.5 GHz, indicating that the shell is resolved at the highest frequency. The shell structure and the size of the outer radius, ~1.0 pc. suggest that this is an evolved H II region. The shell is broken to the south, and the 1.5 and 5 GHz maps suggest that ionized gas may be outflowing in that direction.

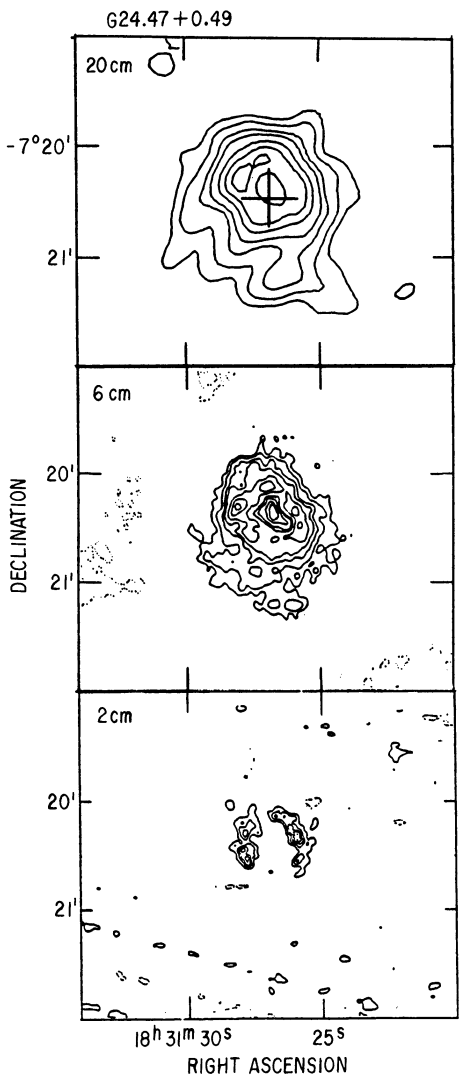

FIG. 7.—VLA radio continuum maps of G24.47+0.49. *Upper panel:* 1.5 GHz map with 14″ resolution. Contour levels are −5, 5, 10, 20, 30, 50, 70, and 90% of the peak flux density of 0.348 Jy beam^{-1}. *Middle panel:* 4.9 GHz map with 4″ resolution. Contour levels are −5, 5, 10, 20, 30, 50, 70, and 90% of the peak flux density of 0.063 Jy beam^{-1}. *Lower panel:* 15 GHz map with 3″ resolution. Contour levels are −1, 1, 2, 3, 4, 5, and 6 times 4 mJy beam^{-1}.

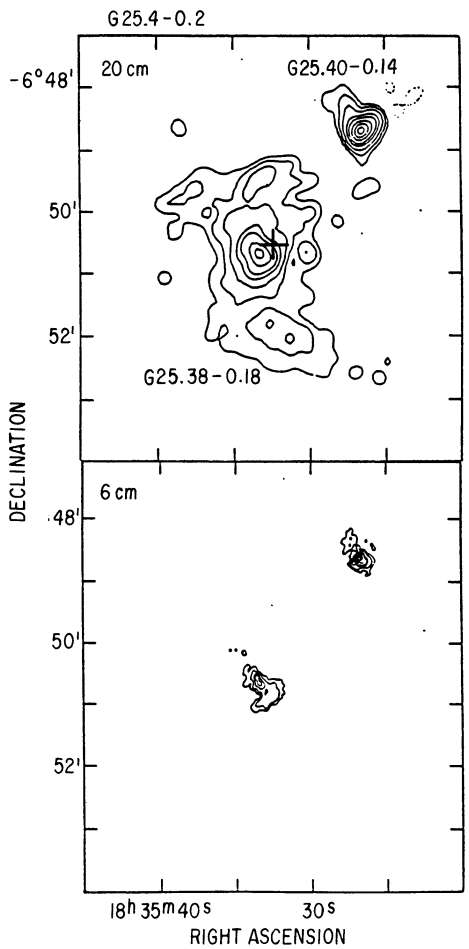

FIG. 8.—VLA radio continuum maps of G25.4−0.2. *Upper panel:* 1.5 GHz map with 14″ resolution. Contour levels are −2.5, 2.5, 5, 10, 20, 30, 50, 70, and 90% of the peak flux density of 1.144 Jy beam^{-1}. *Lower panel:* 4.9 GHz map with 4″ resolution. Contour levels are −5, 5, 10, 20, 30, 50, 70, and 90% of the peak flux density of 0.451 Jy beam^{-1}.

4.8. *G25.4−0.2*

Our VLA map at 1.5 GHz, made with an angular resolution of 14″, shows that G25.4−0.2 consists of two components: (1) an extended source, G25.38−0.18, located toward the center of the map, and (2) a bright source, G25.40−0.14, located ∼2.5 northwest of the main component. The physical relation between these two components is not clear, and it is possible that they may be at substantially different distances. The total flux density in our 1.5 GHz map, 13.1 Jy, is lower than the flux densities measured with a single dish (19.1 Jy at 5 GHz [Downes et al. 1980, 2.6 HPBW]; 16.4 Jy at 36.6 GHz [Berulis & Sorochenko 1973, 1.9 HPBW]), indicating that some of the emission is resolved.

G25.38−0.18 exhibits a core-halo structure. The envelope has an angular size of ∼3′ (∼9 pc at the distance of 10.8 kpc derived by Churchwell, Walmsley, & Cesaroni 1990a), suggesting that this object corresponds to a giant H II complex and not to a compact H II region. The total flux density measured at 1.5 GHz, 10.6 Jy, requires an ionizing flux of 9.8×10^{49} s^{-1}. This result strongly suggests that G25.38−0.18 contains and is excited by a cluster of O and B stars. The core structure is best appreciated in the 5 GHz map (see Fig. 8) in which we resolved out most of the extended emission. This map is in good agreement with that of Woodward, Helfer, & Pipher (1985), who suggested that the core is actually a bipolar H II region. The flux density in our 5 GHz map, 3.2 Jy, is, however, ∼70% higher than the flux density contained in Woodward et al.'s map.

The northwestern source, G25.40−0.14, has a substantial optical depth at 1.5 GHz. The observed peak brightness temperature of 3350 K implies an optical depth of ∼0.4. The radio morphology (see Fig. 8) suggests that this source consists of a

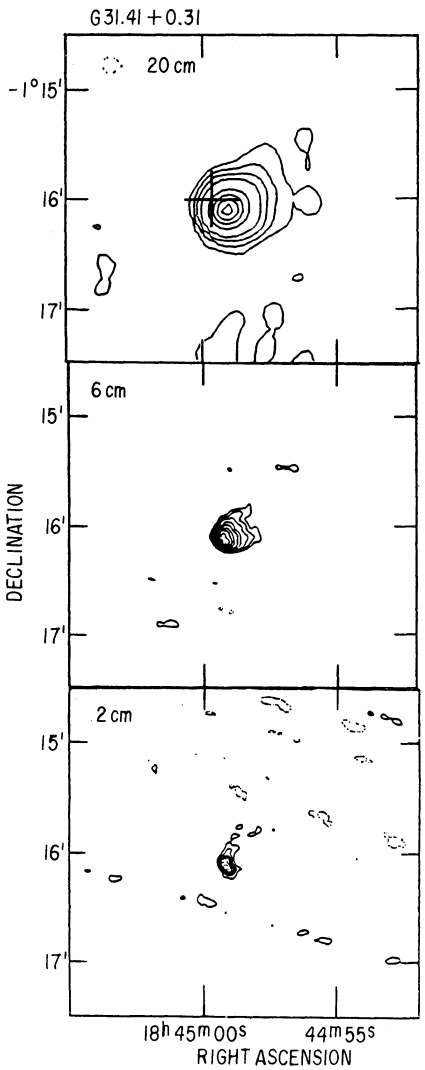

FIG. 9.—VLA radio continuum maps of G31.41+0.31. *Upper panel:* 1.5 GHz map with 14″ resolution. Contour levels are −1, 1, 2.5, 5, 10, 30, 50, 70, and 90% of the peak flux density of 0.589 Jy beam^{-1}. *Middle panel:* 4.9 GHz map with 4″ resolution. Contour levels are −2.5, 2.5, 5, 10, 20, 30, 50, 70, and 90% of the peak flux density of 0.194 Jy beam^{-1}. *Lower panel:* 15 GHz map with 3″ resolution. Contour levels are −15, 15, 30, 45, 60, 75, and 90% of the peak flux density of 0.075 Jy beam^{-1}.

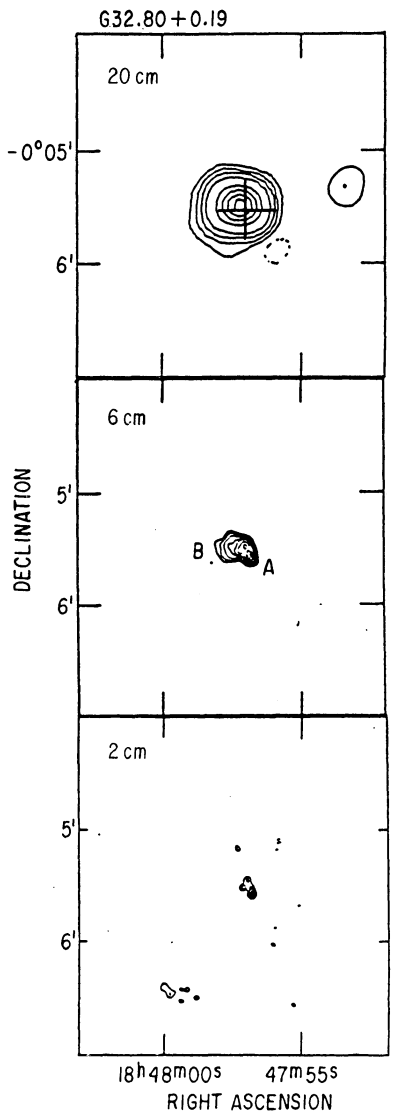

FIG. 10.—VLA radio continuum maps of G32.80+0.19. *Upper panel:* 1.5 GHz map with 14″ resolution. Contour levels are −1, 1, 2.5, 5, 10, 30, 50, 70, and 90% of the peak flux density of 0.907 Jy beam^{-1}. *Middle panel:* 4.9 GHz map with 4″ resolution. Contour levels are −2.5, 2.5, 5, 10, 20, 30, 50, 70, and 90% of the peak flux density of 0.726 Jy beam^{-1}. *Lower panel:* 15 GHz map with 2″ resolution. Contour levels are −10, 10, 20, 30, 50, 70, and 90% of the peak flux density of 0.705 Jy beam^{-1}.

bright central component of ~9″ in size (~0.42 pc in diameter at the distance of 9.6 kpc) and a weak, low brightness temperature component toward the northeast. The total flux density in our 5 GHz map, 4.4 Jy, is considerably larger than that measured by Krassner et al. (1983).

4.9. *G31.41+0.31*

Our VLA maps, especially that at 5 GHz, show that G31.41+0.31 has a cometary-like morphology, exhibiting a compact head toward the east and a tail trailing to the northwest, in good agreement with previous observations at 15 GHz by Gaume & Mutel (1987). Wood & Churchwell (1989) observed this source, with the VLA at 5 GHz and an angular resolution of 0.″4, resolving out most of the emission from the extended tail; ~36% of the total flux density measured by us is contained in their map.

4.10. *G32.80+0.19*

The H II region G32.80+0.19 was previously mapped at 2.7 and 8.1 GHz by WAM. Our VLA maps at 4.9 and 15 GHz show that it consists of at least two components (labeled A and B in Fig. 10). Source A is the brightest (T_b ~ 2200 K at 4.9 GHz) and most compact (diameter ~0.11 pc) component. Source B has a cometary-like morphology, exhibiting a compact head, located ~6″ to the northeast of A, and an extended tail trailing toward the east. At 15 GHz component B is considerably resolved; we detected emission only from the head structure with a flux density of 1.21 Jy.

4.11. *G33.91+0.11*

Our observations show that this source has a core-halo structure, in agreement with the results of WAM, who mapped

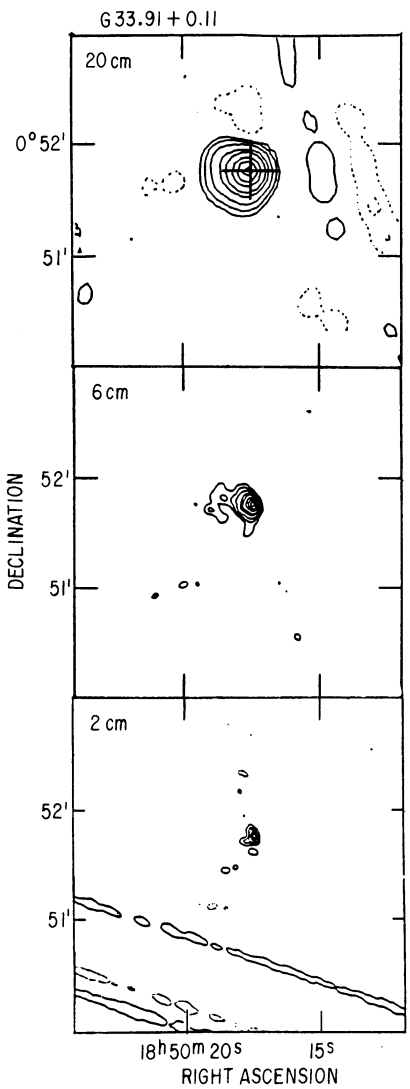

FIG. 11.—VLA radio continuum maps of G33.91+0.11. *Upper panel:* 1.5 GHz map with 13″ resolution. Contour levels are −2.5, 2.5, 5, 10, 20, 30, 50, 70, and 90% of the peak flux density of 0.505 Jy beam^{-1}. *Middle panel:* 4.9 GHz map with 4″ resolution. Contour levels are −2.5, 2.5, 5, 10, 20, 30, 50, 70, and 90% of the peak flux density of 0.297 Jy beam^{-1}. *Lower panel:* 15 GHz map with 3″ resolution. Contour levels are −10, 10, 20, 30, 50, 70, and 90% of the peak flux density of 0.151 Jy beam^{-1}.

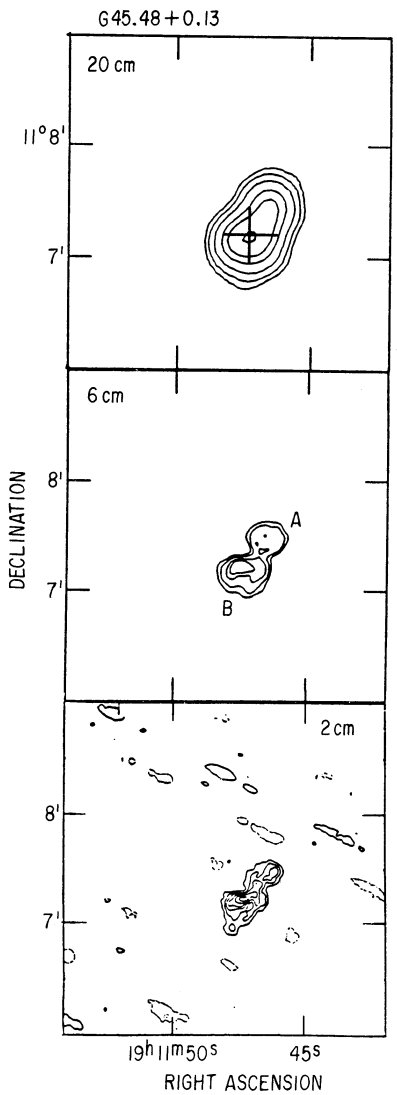

FIG. 12.—VLA radio continuum maps of G45.48+0.13. *Upper panel:* 1.5 GHz map with 17″ resolution. Contour levels are −2.5, 2.5, 5, 10, 20, 30, 50, 70, and 90% of the peak flux density of 1.054 Jy beam^{-1}. *Middle panel:* 4.9 GHz map with 5″ resolution. Contour levels are −5, 5, 10, 20, 30, 50, 70, and 90% of the peak flux density of 0.209 Jy beam^{-1}. *Lower panel:* 15 GHz map with 3″ resolution. Contour levels are −1, 1, 2, 3, 4, 5, 6, and 7 times 5 mJy beam^{-1}.

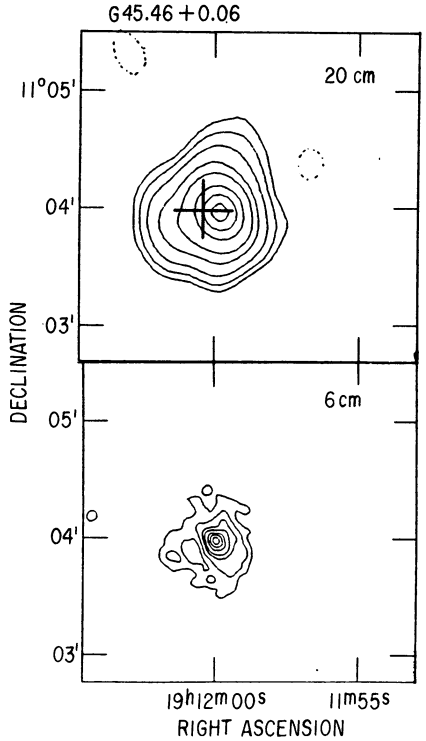

FIG. 13.—VLA radio continuum maps of G45.46+0.06. *Upper panel:* 1.5 GHz map with 17″ resolution. Contour levels are −2.5, 2.5, 5, 10, 20, 30, 50, 70, and 90% of the peak flux density of 1.054 Jy beam^{-1}. *Lower panel:* 4.9 GHz map with 5″ resolution. Contour levels are −5, 5, 10, 20, 30, 50, 70, and 90% of the peak flux density of 0.209 Jy beam^{-1}.

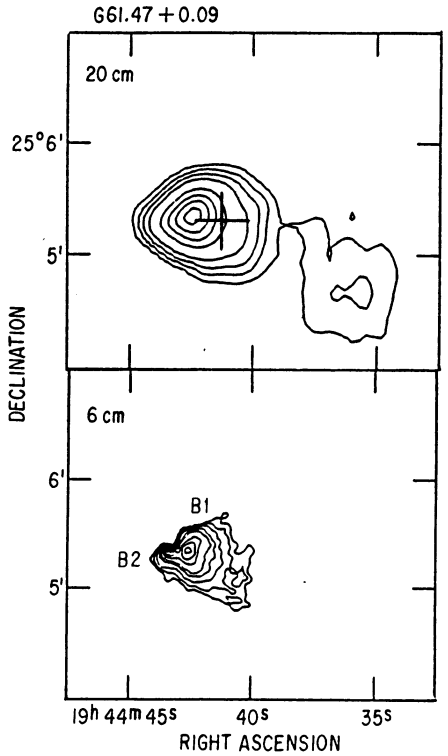

FIG. 14.—VLA radio continuum maps of G61.47+0.09. *Upper panel:* 1.5 GHz map with 14″ resolution. Contour levels are −1, 1, 2.5, 5, 10, 30, 50, 70, and 90% of the peak flux density of 1.382 Jy beam^{-1}. *Lower panel:* 4.9 GHz map with 4″ resolution. Contour levels are −2.5, 2.5, 5, 10, 20, 30, 50, 70, and 90% of the peak flux density of 0.319 Jy beam.

this source at 2.7 and 8.1 GHz with resolutions of 10″ and 4″, respectively. The envelope has a diameter of ∼0.43 pc, while the core has a size of ∼0.16 pc. The total flux density contained in our 5 GHz map, 1.09 Jy, is in good agreement with the flux density of 1.2 Jy measured by WAM at 8.1 GHz, but is 3 times as high as the flux density at 5 GHz measured by Wood & Churchwell (1989) with higher (0.″4) angular resolution.

4.12. *G45.48+0.13 and G45.46+0.06*

G45.48+0.13 and G45.46+0.06 are part of a group of H II regions near $l = 45°$, $b = 0°$, which were mapped interferometrically at 1.4 and 5 GHz with the WSRT by Matthews et al. (1977).

Our VLA maps (see Fig. 12) show that G45.48+0.13 has a bipolar structure, exhibiting a southern lobe of ∼17″ in diameter (component B) and a northern lobe of ∼13″ in diameter (component A), separated by ∼20″. The total flux density contained in our 5 GHz map, 1.33 Jy, is lower than the flux density, of 1.93 Jy, measured by Matthews et al. (1977). Wood & Churchwell (1989) observed the southern component of G45.48+0.13 with an angular resolution of 0.″4 resolving out most of the emission; their map at 5 GHz, which shows an irregular, multiple-peaked structure, contains only ∼25% of the total flux density measured by us. We suggest that the bipolar morphology of the H II region might be produced by the presence of a massive circumstellar disk around the exciting star. Support for this suggestion is provided by the presence of an OH maser located between the two lobes (Goss et al. 1973). Alternatively, the observed radio structure might be due to the superposition in the plane of the sky of two unrelated H II regions. The total number of ionizing photons per second needed to excite the bipolar source, 4.4×10^{48} s^{-1}, could be supplied by an O7 ZAMS star.

Our VLA maps at 1.5 and 5 GHz (see Fig. 13) show that G45.46+0.06 exhibits a core-halo structure. The integrated flux density contained in our 5 GHz map is 4.02 Jy, which is about 60% smaller than the value measured by Matthews et al. (1977). Wood & Churchwell (1989) observed G45.46+0.06 at 5 GHz with an angular resolution of 0.″4, detecting an ultracompact source, classified as a cometary shape, having a flux density of ∼10% of the total flux density measured by us.

4.13. *G61.47+0.09*

This source was previously mapped at 5 GHz with the WSRT by Felli & Harten (1981). Our VLA map at 5 GHz (see Fig. 14) shows that G61.47+0.09 (or S88B) consists of an extended cometary-like region of ionized gas, with a flux density of 4.36 Jy and a size of ∼0.44 pc (component S88B1), and a bright ultracompact source, with a flux density of 0.83 Jy and a size of ∼0.16 pc, at the eastern edge of the main region (component S88B2).

In the high angular resolution (0.″4) VLA observations of G61.47+0.09 by Wood & Churchwell (1989), the emission from the extended cometary-like H II region is almost entirely resolved out; the source has an irregular multiple-peaked structure with a total flux density of 0.21 Jy. The eastern source is also partially resolved out.

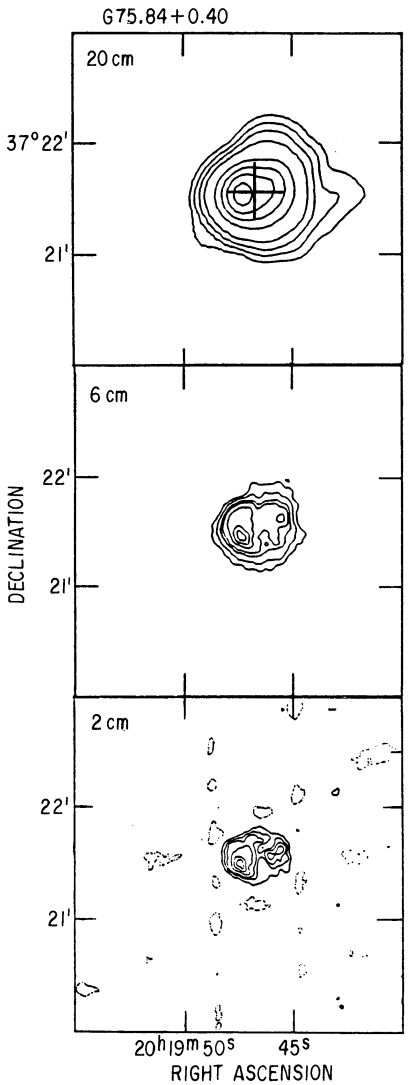

FIG. 15.—VLA radio continuum maps of G75.84+0.40. *Upper panel:* 1.5 GHz map with 14″ resolution. Contour levels are −1, 1, 2.5, 5, 10, 30, 50, 70, and 90% of the peak flux density of 1.493 Jy beam^{-1}. *Middle panel:* 4.9 GHz map with 4″ resolution. Contour levels are −5, 5, 10, 20, 30, 50, 70, and 90% of the peak flux density of 0.327 Jy beam^{-1}. *Lower panel:* 15 GHz map with 3″ resolution. Contour levels are −10, 10, 20, 30, 50, 70, and 90% of the peak flux density of 0.129 Jy beam^{-1}.

At 1.5 GHz, we detected toward the west of G61.47+0.09 a source of very low brightness temperature (see Fig. 14). It probably corresponds to an old and evolved H II region. The whole appearance of the H II region complex, exhibiting an extended and presumably evolved H II region toward the west, a smaller (0.22 pc in radius) region of ionized gas toward the center, and a compact, presumably young, region of ionized gas toward the east, might suggest a sequential formation of the H II regions.

4.14. *G75.77+0.34 and G75.84+0.40*

G75.77+0.34 and G75.84+0.40 are part of the H II complex associated with the OH maser source ON-2 (Hardebeck & Wilson 1971). The whole complex has been mapped interferometrically with the WSRT at 1.4 GHz (Matthews et al. 1977) and at 5 GHz (Matthews et al. 1973).

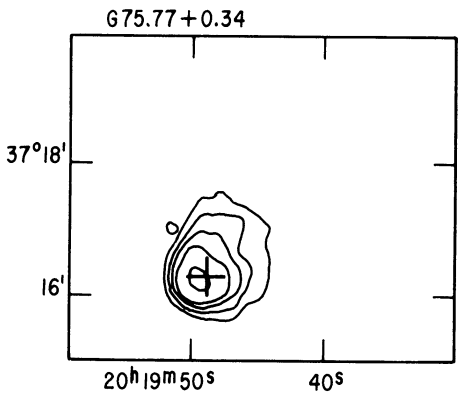

FIG. 16.—VLA radio continuum map at 1.5 GHz of G75.77+0.34 with 14″ resolution. Contour levels are −0.015, 0.015, 0.037, 0.075, 0.15, and 0.45 Jy beam^{-1}.

A likely model for the morphology of G75.8+0.4, based on our VLA maps and the 5 GHz map of Harris (1976), is that of an inhomogeneous shell of gas ionized by a single central star. The outer radius of the shell, measured from the 10% contour level in the 15 GHz map, is ∼17″ (∼0.34 pc at 4.1 kpc). The optical depth at 1.5 GHz is ∼0.55. Wood & Churchwell (1989) observed, with an angular resolution of 0.″4, the eastern side of the shell, detecting about 10% of the flux density measured by us. Their results suggest that the shell has a clumpy structure.

Our VLA map at 1.5 GHz (see Fig. 16) shows that G75.77+0.34 has a cometary-like morphology. The flux density we measured at 1.5 GHz, 4.73 Jy, is higher than the flux density, 3.2 Jy, measured by Harris (1976) at 1.4 GHz. Matthews et al. (1973) measured flux densities of 3.0 and 5.1 Jy at 5 and 10.7 GHz, respectively. To the northeast of this source lies the ultracompact H II region G75.87+0.34 which is associated with the OH source ON-2 (Hardebeck & Wilson 1971).

5. DISCUSSION

5.1. *Radio Continuum Morphologies*

Of the 16 *IRAS* point sources investigated here, nine (G1.13−0.11, G13.87+0.28, G23.87−0.12, G24.47+0.49, G31.41+0.31, G33.91+0.11, G45.48+0.13, G75.77+0.34, and G75.84+0.40) are associated with regions of ionized gas that have simple structure. Hereafter we will refer to these objects as the simple H II regions. Their most common morphologies are shell (three sources) and cometary (three sources) shapes. Mechanisms that may create and maintain these types of structures have been discussed by Wood & Churchwell (1989) and by Van Buren et al. (1990). The spectral types of the stars exciting the simple H II regions are distributed in a narrow range between O7 and O5.5. This distribution is, however, statistically unsuitable to determine the initial mass function for massive stars, since our sample is highly biased toward the strongest IR and radio sources and thus contains preferentially the objects with the higher luminosities. We may conclude, however, that stars with spectral types earlier than O5 are very rare.

Seven *IRAS* sources (G9.61+0.20, G7.47+0.06, G32.80+0.19, G61.47+0.09, G10.5+0.0, G25.4−0.2, and G45.46+0.06) are associated with regions of ionized gas that have complex radio continuum structure. Thus, it appears that ∼45% of the *IRAS* point sources associated with unresolved (by single dish) H II regions are excited by more than one star.

High angular resolution radio continuum observations of these objects are required to delineate their structure and to determine the physical properties of the ionized gas and the characteristics of the exciting star(s). For instance, the spectral types derived by Chini et al. (1986a, b) assuming that the total infrared luminosity is provided by a single star correspond to upper limits.

The regions of ionized gas studied here are not homogeneous in density. Seven of the H II regions in our sample were observed by Wood & Churchwell (1989), with an angular resolution about 10 times better than ours (beam 10 times smaller), resolving out a considerable fraction of the emission detected in the present observations. Their maps usually exhibit multiple-peaked irregular structures and ultracompact components. These small structures might be density inhomogeneities within the larger H II region. In this picture, the compact structures are externally ionized. If completely ionized, the clumps must exist close to the edge of the H II region (Ho & Haschick 1981) and may reflect the clumpy structure of the neutral material into which the H II region is expanding. Alternatively, the clumps may be partially ionized dense globules within the H II region, produced by the fragmentation of the accreting molecular gas that collapsed to form the central exciting star. It is also possible that some objects could be ultracompact H II regions embedded in molecular gas associated with larger diffuse H II regions formed by earlier episodes of massive star formation.

Our observations support the conventional wisdom that compact H II regions are usually found in groups (Habing & Israel 1979). Only five (G1.13−0.11, G13.87+0.28, G24.47+0.49, G31.41+0.31, and G33.91+0.11) of the nine simple sources appear completely isolated. The remaining four simple sources (G45.48+0.13, G23.87−0.12, G75.77+0.34, and G75.84+0.40) are close to other H II regions. The large fraction of complex regions in our sample and that of Wood & Churchwell indicates the gregarious nature of compact H II regions. Extreme clustering is seen toward two complex regions (G10.5+0.0 and G25.4−0.2), which are themselves near other complex H II regions, suggesting that multiple clusters of OB stars may have formed in these regions.

5.2. *Distances*

Accurate distances are essential for the determination of physical parameters of compact H II regions. In this paper we adopt, wherever possible, the distances given by Churchwell et al. (1990a), derived from the ammonia line velocities and the rotation curve of Brand (1986), except for source G7.47+0.06, for which we adopt the distance derived by WAM. Only one of our sources, G9.61+0.20, is not included in the Churchwell et al. (1990a) sample. Its distance is poorly known; Downes et al. (1980) could not resolve the distance ambiguity. Kurtz, Churchwell, & Wood (1993) derived near and far kinematic distances of 0.6 and 16.1 kpc, respectively.

A possible way to resolve the near-far distance ambiguity arises from the comparison of the stellar luminosity required to maintain ionization of the H II region in the absence of dust (L_{UV}) with the total FIR luminosity (L_{FIR}). In no circumstances should the L_{UV}/L_{FIR} ratio be greater than unity. In columns (3) and (4) of Table 5 we give L_{UV} and L_{FIR} for all sources in our sample. L_{UV} was derived from the relationship between the ionizing flux and the stellar luminosity given by Panagia (1973), with the rate of ionizing photons calculated using the radio continuum flux densities given in Tables 2 and 3 (see eq. [1]). The total FIR luminosities are taken from Chini et al. (1987), corrected to the distances given in column (2). For all sources, except G9.61+0.20 and G7.47+0.06, the L_{UV}/L_{FIR} ratios are less than unity, ranging from 0.27 to 0.79 and having an average value of 0.5. Possible explanations of the ratios being smaller than unity involves (1) the presence of dust within the H II region and (2) excitation by a cluster of stars. In the first possibility the ionizing stellar photons are absorbed by the dust and hence L_{UV} underestimates the luminosity of the star. The second explanation assumes that L_{FIR} includes the luminosity of stars that do not produce a considerable amount of ionizing photons and hence that L_{FIR} overestimates the luminosity of the exciting star. Both of these possibilities will be discussed further in § 5.4.

TABLE 5

LUMINOSITY OF THE EXCITING STARS

Source (1)	D (kpc) (2)	L_{UV} ($10^5\ L_\odot$) (3)	L_{FIR} ($10^5\ L_\odot$) (4)	L_{UV}/L_{FIR} (5)
G1.13−0.11	8.5	2.7	7.0	0.39
G7.47+0.06	6.3	2.5	1.1	2.2
G9.61+0.20	0.6	0.35	0.05	7.0
	16.1	6.0	36	0.17
G10.5+0.0	5.8	2.0	4.3	0.45
G13.87+0.28	4.4	1.5	2.2	0.67
G24.47+0.49	9.4	4.9	15	0.32
G23.87−0.12	10.6	2.2	4.1	0.55
G25.38−0.18	10.8	13	32	0.41
G31.41+0.31	7.9	1.3	2.4	0.56
G32.80+0.19	13.0	8.9	18	0.51
G33.91+0.11	8.3	1.5	3.3	0.45
G45.48+0.13	6.0	1.1	3.8	0.27
G45.46+0.06	6.6	3.0	6.9	0.44
G61.47+0.09	5.4	3.0	7.4	0.40
G75.84+0.40	4.1	2.6	3.4	0.79
G75.77+0.34	4.1	1.3	2.4	0.55

For G9.61+0.20 we find that L_{UV}/L_{FIR} is either 7 or 0.17, depending on whether the source is at the near or far kinematic distance, respectively. This result suggests that G9.61+0.20 is probably at the far kinematic distance. The reason why a shift to the far distance produces a decrease in L_{UV}/L_{FIR} is that while L_{FIR} and the number of ionizing photons are proportional to distance squared, L_{UV} depends on distance to a power lower than 2 (Churchwell et al. 1990a). Similarly, the L_{UV}/L_{FIR} ratio derived for G7.47+0.06 suggests that this source may be at a farther distance than the assumed 6.3 kpc.

5.3. *Density versus Size Relationship*

A large fraction (about 70%) of the objects in our sample have diameters between 0.1 and 1 pc and electron densities between 10^3 and 10^4 cm^{-3}, corresponding to compact H II regions of class II in the classification scheme of Habing & Israel (1979).

Figure 17 shows a plot of the electron density against the diameter for all the H II regions in our sample (*circles*) and for the compact and ultracompact regions of the sample of Wood & Churchwell (1989) (*crosses*). There is a strong correlation between these two physical parameters. A least-squares fit to the function $\langle N_e^2\rangle^{1/2} = a \log D + b$, using data from both samples, gives $a = -0.98 \pm 0.04$ and $b = 3.03 \pm 0.05$. Drawn in Figure 17 are the fitted relation and a line with a constant excitation parameter (or constant number of ionizing photons).

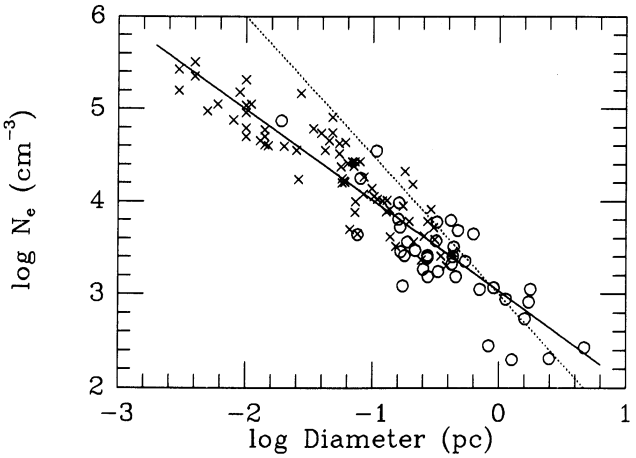

FIG. 17.—Plot of rms electron density vs. linear diameter for compact and ultracompact H II regions. Crosses correspond to H II regions from the sample of Wood & Churchwell (1989); open circles correspond to the H II regions analyzed in this paper. The continuous line is a least-squares fit to the data. The dashed curve corresponds to a line of constant number of ionizing photons ($N_i = 1.3 \times 10^{49}$ s^{-1}).

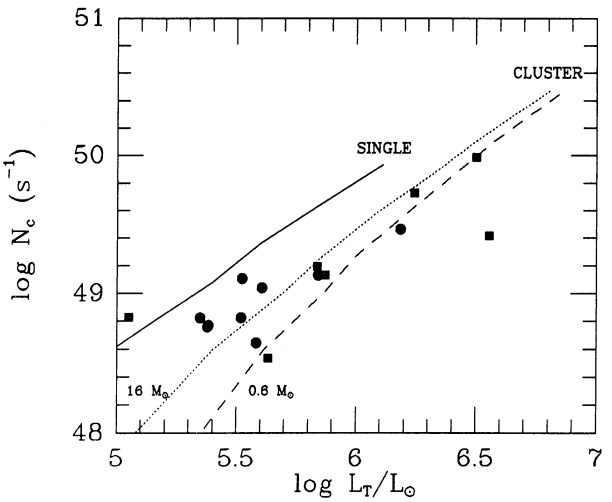

FIG. 18.—Number of ionizing photons vs. IR luminosity diagram. Filled circles and squares correspond to the simple and complex H II regions, respectively. The lines correspond to theoretical curves for single stars (*solid line*) and for cluster of stars. The dotted and dashed curves represent computations made assuming that the cluster has an initial mass function as given by Miller & Scalo (1979) and a minimum stellar mass of 16 and 0.6 $M_\odot$, respectively.

If the distribution of the spectral types (or ionization characteristics) of the stars exciting H II regions is independent of the initial conditions of the surrounding medium, one expects to find that on average $N_e \propto D^{-1.5}$. A possible explanation for the less steep observed power-law index is that on the average ultracompact H II regions are excited by stars with lower luminosities (thus lower numbers of ionizing photons) than those exciting less compact H II regions. An alternative interpretation, which we suggest as more probable, is that several of the ultracompact H II regions of Wood & Churchwell (1989) might correspond to the most dense structures within an inhomogeneous H II region excited by a single luminous star. In this case, the number of ionizing photons exciting the compact source is smaller than the actual number of ionizing photons emitted by the star. Support for this suggestion is provided by the comparison of our observations with those of Wood & Churchwell as (1989) as discussed in § 5.1.

5.4. *Single- or Multiple-Star Excitation?*

The radio morphology of the complex sources suggests that they are excited by multiple stars. Even for the simple sources it is possible that a cluster, rather than a single star, may be responsible for the total IR luminosity. Because the resolution of *IRAS* at 60 and 100 μm wavelengths is $\geq 2'$, the FIR observations may include several less massive stars in an association that will contribute to the FIR luminosity but that are not hot enough to contribute to ionization. To investigate this possibility, we compare the FIR luminosities and the total rate of ionizing photons needed to excite the H II complex, $N_c'^{\rm TOT}$, derived from the radio observations.

Figure 18 shows theoretical relations between the number of ionizing photons and the total luminosity both for single stars (Panagia 1973) and for a cluster of stars. To compute the latter, it is necessary to assume an initial mass function and then compute the number of ionizing photons, $N_c^{\rm cl}$, emitted by a cluster with a given total luminosity. The long-dashed line in Figure 18 represents the result from a model calculation obtained by adopting the Miller & Scalo (1979) initial mass function and assuming that the minimum stellar mass in the cluster is 0.6 $M_\odot$. For a given total luminosity, the most luminous star in the cluster hypothesis is typically between three and four subclasses cooler than that inferred from the single-star assumption (*continuous line*).

Also plotted in Figure 18 are $N_c'^{\rm TOT}$ versus the total IR luminosity for all objects in our sample. $N_c'^{\rm TOT}$ corresponds to the sum of N_c' over all of the individual components within a source, where N_c' is the rate of Lyman continuum photons required to excite a single component. The later is computed from the observed radio flux density using the relation (cf. Moran 1983)

$$N_c' = 7.6 \times 10^{46} \left(\frac{S_\nu}{\rm Jy}\right)\left(\frac{T_e}{10^4\ {\rm K}}\right)^{-0.45}\left(\frac{D}{\rm kpc}\right)^2\left(\frac{\nu}{\rm GHz}\right)^{0.1} {\rm s}^{-1}\,. \quad (1)$$

Values for the simple sources are plotted as circles, while values for the complex sources are plotted as squares. As seen in Figure 18, most of the observed points fall between the single and the cluster model relations.

The multiple-star model which assumes that the cluster contains the whole spectrum of masses up to 0.6 $M_\odot$, besides not explaining the observations, faces a potential difficulty concerning stellar densities. For instance, for a total luminosity of 7×10^5 $L_\odot$, typical of the sources in our sample, the cluster model implies the presence of ~ 5600 member stars with spectral types earlier than K5. At the distances of the sources studied here the linear size of the beam at 100 μm is typically ~ 9 pc; thus the volume sampled by the FIR observations is ~ 330 pc^3. The density of stars with masses greater than 0.6 $M_\odot$ implied by this particular cluster model is then ≥ 20 stars pc^{-3}. This is a large stellar density, 2–10 times higher than that derived in the central (~ 7 pc) regions of Galactic open clusters (cf. Herbig 1982).

Assuming that the dust within the region of ionized gas does not play a role, the multiple-star model that best explains the observations is one in which the cluster contains only massive stars (see the dotted curve in Fig. 18, which corresponds to a

cluster model with a minimum mass of 16 $M_\odot$, namely, stars with spectral types earlier than B1). Bimodal star formation, where high-mass stars (early OB) and low-mass stars (late B or later) are formed under independent processes, has been proposed by Güsten & Mezger (1983), Shu, Adams, & Lizano (1987), and others.

To omit the role of dust is, nevertheless, unjustified. The actual location of our sources in the $L_{\rm FIR}$ versus $N_c'^{\rm TOT}$ diagram is most probably dictated both by the presence of dust within the H II regions and by excitation from several stars. It is not easy, however, to disentangle which of these causes produces the predominant effect. Nevertheless, we argue that for the complex sources, based on their large IR luminosities, typically 3 times more luminous than the simple sources, and on their morphologies, the presence of multiple stars is the main factor responsible for their IR and radio characteristics. Several arguments for multiple OB star formation within a region a few parsecs in extent have been presented by Ho & Haschick (1981). On the other hand, for the simple sources we will assume that the role of dust is the predominant one.

5.5. *Characteristics of the Infrared-emitting Region*

Compact H II regions are among the brightest and most luminous objects in the Galaxy at infrared wavelengths. The IR emission, well in excess of the expected free-free radiation, is presumably thermal emission arising from dust in and around the ionized gas. Dust absorbs nearly all of the stellar radiation and reemits it in the infrared. Thus, if the distance to a particular source is known, the total luminosity of the central exciting star (or cluster of stars) can be determined from the integrated infrared flux density.

5.5.1. *Dust Surrounding the* H II *Region*

Flux densities over the entire infrared region of the electromagnetic spectrum, from wavelengths ranging from 1 to 1300 μm, have been measured for most of the sources studied in the present work (Chini et al. 1987). By fitting a modified Planck curve to the observations at the longest wavelength range (100–1300 μm), Chini et al. (1986b) derived a mean temperature of 26 K. This corresponds to the average temperature of the large and cool dust cloud far from the central star. The flux densities observed at 12 and 25 μm are, however, well above the fitted curve, indicating that the emission at these wavelengths arises from warmer dust.

The 12 μm/25 μm and 12 μm/20 cm ratios of flux densities are quite similar for all objects in our sample. Figure 19 shows the 12 μm flux density plotted against the integrated 20 cm flux density and against the 25 μm flux density. There is a clear relationship between the flux densities at these wavelengths. Least-squares fits to the functions $S_{12\,\mu\rm m} = CS_{20\,\rm cm}$ and $S_{12\,\mu\rm m} = DS_{25\,\mu\rm m}$ give $C = 23.6 \pm 1.7$ and $D = 0.122 \pm 0.010$. The small scatter in the flux density ratios indicates that the physical conditions of the warm dust region are similar from object to object.

Assuming a simple model in which the radio emission at 20 cm arises from a uniform optically thin region of ionized gas with an electron temperature T_e and that the 12 and 25 μm emission arises mainly from an optically thin uniform region of warm dust embedded within a large cloud of cool gas, then the 12 μm/25 μm and 12 μm/20 cm flux density ratios are given by

$$\left(\frac{S_{12\,\mu\rm m}}{S_{25\,\mu\rm m}}\right) = \left[\frac{B_{12\,\mu\rm m}(T_{\rm wd})}{B_{25\,\mu\rm m}(T_{\rm wd})}\right]\left(\frac{25}{12}\right)^n \exp\left\{-\left[1-\left(\frac{12}{25}\right)^n\right]\tau^C_{12\,\mu\rm m}\right\}, \quad (2)$$

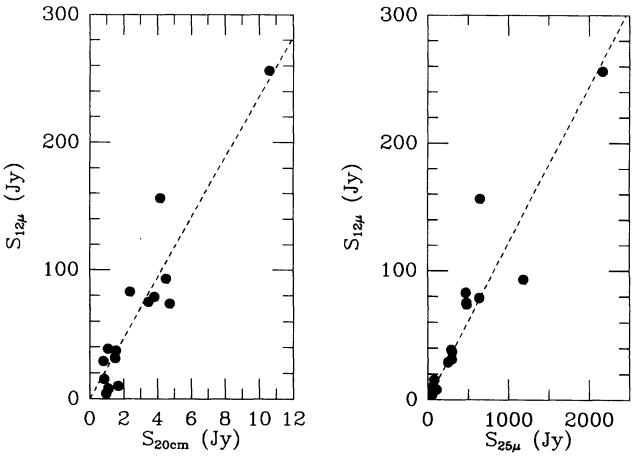

FIG. 19.—Plot of the 12 μm flux density vs. the integrated 20 cm radio flux density (*left*) and the 25 μm flux density (*right*). The dashed lines are least-squares fits to the data.

and

$$\left(\frac{S_{12\,\mu\rm m}}{S_{20\,\rm cm}}\right) = \left[\frac{B_{12\,\mu\rm m}(T_{\rm wd})}{B_{20\,\rm cm}(T_e)}\right]\left(\frac{\tau^H_{12\,\mu\rm m}}{\tau_{20\,\rm cm}}\right)\exp\left(-\tau^C_{12\,\mu\rm m}\right), \quad (3)$$

where $T_{\rm wd}$ is the temperature of the warm dust; B_ν is the Planck function; $\tau^H_{12\,\mu\rm m}$ and $\tau^C_{12\,\mu\rm m}$ are, respectively, the optical depths at 12 μm of the warm dust region and of the cold dust cloud in front of it; and $\tau_{20\,\rm cm}$ is the optical depth of the ionized gas at 20 cm. In writing expression (3), we have implicitly assumed that the ratio of solid angles of the warm dust and ionized gas regions is equal to unity. This somewhat crude assumption may be justified by the good agreement between the 20 μm and radio continuum maps observed toward similar regions (Haschick & Ho 1983). In addition, in equation (2) we have used the common approximation,

$$\frac{\tau_{\lambda_1}}{\tau_{\lambda_0}} = \left(\frac{\lambda_0}{\lambda_1}\right)^n. \quad (4)$$

that relates the opacities of the dust at infrared wavelengths (Hildebrand 1983). The index n depends on the wavelength, and ranges from 1 to 2 (cf. Cox & Mezger 1989).

Given T_e, $\tau_{20\,\rm cm}$, and $\tau^C_{12\,\mu\rm m}$, expressions (2) and (3) can be used to derive the temperature and the 12 μm opacity of the warm dust cloud. The 12 μm opacities of the cool dust clouds associated with the H II regions studied here are not known and are difficult to estimate. From model calculations of the emission from dust cocoons around newly formed stars, which fit the whole observed spectrum, Churchwell et al. (1990b) predict 12 μm optical depths of $\sim$2 for the cool (26 K) cloud. In the following we derive physical parameters of the warm dust around the compact H II regions using the average value of the observed quantities among all objects in our sample. Accordingly, these parameters should only be taken as representative of the class as a whole. A detailed calculation for each source is beyond the scope of this paper. Using $S_{12\,\mu\rm m}/S_{20\,\rm cm} = 23.6$, $S_{12\,\mu\rm m}/S_{25\,\mu\rm m} = 0.122$, and $\tau_{20\,\rm cm} = 0.3$ (i.e., the average of the observed values), $n = 1$, and $T_e = 10^4$ K, we find that, for $\tau^C_{12\,\mu\rm m}$ in the range 1–3, $T_{\rm wd}$ is in the range 140–180 K, and that $\tau^H_{12\,\mu\rm m}$ is $\sim$0.003. These dust temperatures are similar to the temperature of molecular gas immediately surrounding

TABLE 6

FIR AND RADIO CONTINUUM PROPERTIES OF SIMPLE SOURCES

		FIR		RADIO			IRE	
SOURCE (1)	D (kpc) (2)	L_{FIR} ($10^5\ L_\odot$) (3)	N_c^{*} [a] ($10^{49}\ s^{-1}$) (4)	N_c' ($10^{49}\ s^{-1}$) (5)	$L(Ly\alpha)$ ($10^5\ L_\odot$) (6)	f_d (7)	Observed (8)	Expected (9)
G1.13−0.11	8.5	7.0	4.3	1.35	0.57	0.69	12.2	9.2
G13.87+0.28	4.4	2.2	1.05	0.66	0.28	0.37	7.9	6.3
G24.47+0.49	9.4	15.3	8.51	2.91	1.23	0.66	12.4	7.4
G23.87−0.12A	10.6	4.1	2.34	1.10	0.46	0.53	8.7	6.8
G31.41+0.31	7.9	2.4	1.15	0.59	0.25	0.49	9.7	7.8
G33.91+0.11	8.3	3.3	1.77	0.67	0.28	0.62	11.7	9.4
G45.48+0.13	6.0	3.8	2.17	0.44	0.19	0.80	20.6	16.7
G75.84+0.40	4.1	3.4	1.80	1.28	0.54	0.29	6.2	4.7
G75.77+0.34	4.1	2.4	1.14	0.58	0.24	0.49	9.8	7.9

[a] Assuming that a single star provides the entire infrared luminosity.

compact H II regions, as derived from observations of highly excited lines of ammonia (Keto, Ho, & Haschick 1987; Garay & Rodríguez 1990). Presumably the warm dust and molecular gas are part of the dense neutral shock that surrounds the ionized gas region.

Undoubtedly the characterization of the dust emission as arising from an inner, single-temperature warm dust region surrounded by a large, single-temperature cool cloud is a crude approximation. Model computations to reproduce the observed IR flux distribution require that the dust temperature continuously decrease with the radial distance from the exciting star (Churchwell et al. 1990b). The calculations show that the dust temperature drops very steeply in an inner shell region surrounding the ionized nebula (our warm dust region) and much more slowly farther out where most of the FIR emission is produced (our cold dust region). The two-temperature dust model is thus a reasonable approximation. In fact, the temperatures and opacities derived from our simple model are in good agreement with the more detailed results.

5.5.2. *Dust within the* H II *Region*

In the following discussion of the properties of the dust within H II regions we will consider only the simple (or isolated) sources, and assume that they are excited by a single star. Dust within the ionized gas region should be considerably hotter than the ~150 K dust detected at 12 μm. Its average temperature is probably ~500 K, with a maximum of ~2000 K, the dust sublimation temperature. Thus, the hot dust is expected to emit the bulk of its luminosity at wavelengths of ~1 μm. At these wavelengths, the circumstellar cocoon is, however, optically thick and therefore will absorb most of the radiation from the hot dust. Therefore, unless the dust is very clumpy, we do not expect to see the "hot dust" at near-infrared wavelengths.

The presence of dust within the H II region can, however, be inferred from a comparison of the number of ionizing photons derived from the radio continuum observations (eq. [1]) and from the total luminosity of the exciting star derived from the IR observations (cf. Fazio 1976). Table 6 lists the FIR and radio continuum properties of the simple sources. The total luminosity of the central stars (col. [3]) is derived from the observations of flux densities ranging from 1 to 1300 μm by Chini et al. (1987), using the distances given in column (2). Assuming that the luminosity is provided by a single star, we derive its spectral type and the total rate of Lyman continuum photons, N_c^{*}, emitted by the exciting star (col. [4]) using Panagia's (1973) computations. The number of ionizing photons needed to excite the H II regions, N_c', is given in column (5). The fraction of Lyman continuum photons absorbed by dust within the H II region, f_d, is then simply $1 - (N_c'/N_c^{*})$. Typically, f_d (col. [7]) is 0.5, indicating that in compact H II regions a significant amount of UV photons is absorbed by dust within the ionized gas.

From a similar analysis, but using radio flux densities obtained from interferometric observations with high angular resolution (0".4), Wood & Churchwell (1989) derived values of f_d in the range 0.5–0.9, but most were near 0.9. Their measurements, however, tend to emphasize small, bright, high-density considerations but resolve out the lower density regions in which they are embedded. For five H II regions observed in common by Wood & Churchwell (1989) and by us, we derived f_d values of 0.5 while they found 0.9. The large values derived by Wood & Churchwell (1989) are most likely produced by an underestimation of the total radio luminosity due to the insensitivity of their observations to structures larger than 10".

5.5.3. *Infrared Excess*

The copious amount of infrared energy emitted by the objects considered here naturally raises the question of the source of dust heating. Since in an ionized bounded nebula a substantial fraction of the stellar energy is converted into Lyman-α photons, which are absorbed by the grains in the neutral outer region and within the ionized region, the Lyα radiation is expected to be an important energy source for dust heating. For instance, for old planetary nebula it has been found that the infrared energy can be completely provided by the absorption of nebular Lyα photons (Krishna Swamy & O'Dell 1968; Pottasch et al. 1984). Column (6) of Table 6 gives the Lyα luminosity, $L(Ly\alpha)$, of the simple H II regions in our sample. They were computed from the observed radio continuum flux density using the relation

$$L(Ly\alpha) = 3.20 \times 10^2 \left(\frac{S_\nu}{\mathrm{Jy}}\right)\left(\frac{\nu}{\mathrm{GHz}}\right)^{0.1}\left(\frac{T_e}{10^4\ \mathrm{K}}\right)^{-0.45}\left(\frac{D}{\mathrm{kpc}}\right)^2 L_\odot , \quad (5)$$

assuming that $T_e = 10^4$ K. Comparison with the observed infrared luminosities (see col. [3] of Table 6) shows that the Lyα emission does not contain sufficient energy to heat the

dust. The infrared excesses (IREs), defined as the ratio of the observed infrared luminosity to the Lyα luminosity (given in col. [8] of Table 6), range from 6 to 21, showing that the Lyα emission alone is not able to explain the infrared luminosities. A similar result for other compact H II regions was previously found by Antonopoulou & Pottasch (1987).

In previous sections we assumed that the stellar radiation from the embedded ionizing object is the energy source of all of the infrared emission. It is implicit in this assumption, for instance, that heating by the interstellar radiation field is not important. To be consistent with our assumption, and to reaffirm the value of the parameters derived earlier on, we have then to demonstrate that the infrared excess can be explained within the above hypothesis. Besides absorption of Lyα photons, other mechanisms of dust heating by the central star are direct absorption of Lyman continuum photons by grains within the H II region and absorption of nonionizing photons by grains in both the ionized region and in the surrounding neutral region. Assuming that all the stellar luminosity below the Lyman continuum ($\lambda > 912$ Å) is absorbed by dust in the surrounding molecular cloud, then the expected ratio of infrared luminosity of Lyα luminosity is (Petrosian, Silk, & Field 1972)

$$\frac{L(\mathrm{IR})}{L(\mathrm{Ly}\alpha)} = \left[1 + \frac{1-f}{f}\frac{\langle h\nu\rangle_{\mathrm{Lyc}}}{h\nu_{\mathrm{Ly}\alpha}} + \frac{(1-P)\alpha_\infty}{f}\right], \qquad (6)$$

where $\langle h\nu\rangle_{\mathrm{Lyc}}$ is the average energy of the stellar Lyman continuum photons, $1 - P$ is the fraction of the energy emitted longward of the Lyman continuum edge, α_∞ is the ratio of the total stellar luminosity to the expected Lyα luminosity in the absence of dust, and f is the fraction of Lyman continuum photons absorbed by gas in the ionized region. In writing equation (6) we have further assumed that all the recombinations to the excited levels of hydrogen lead to the emission of a Lyα photon.

The expected IREs for the simple H II regions, computed from equation (6) using $f = 1 - f_d$ with f_d as given in Table 6, $\langle h\nu\rangle_{\mathrm{Lyc}}/h\nu_{\mathrm{Ly}\alpha} = 1.5$, P and α_∞ (taken from Panagia 1973) for a star with N'_c/f ionizing photons, are given in column (9) of Table 6. The theoretical IREs are in good agreement with the observed IREs (derived from the observed flux densities in the 1–1300 μm wavelength range and radio flux density at 20 cm), although they are systematically lower by a factor of 0.8. The theoretical and observed values can be brought into a much better agreement if we take into account that, at the densities of our regions of ionized gas, there is a finite probability that a recombination to the 2s level of hydrogen results in a two-photon emission instead of a Lyα photon emission. We conclude that the observed infrared excesses are therefore explained by the energy of the exciting star. In addition, we conclude that, of the total luminosity emitted by the dust associated with compact H II regions, typically, (1) ~60% corresponds to reprocessed emission from stellar photons longward of the Lyman continuum limit directly absorbed by dust outside the H II region; (2) ~25% comes from radiation reemitted by the hot dust within the H II region; and (3) ~15% is due to heating by Lyα photons.

6. SUMMARY

We made multifrequency, high angular resolution, radio continuum observations, using the VLA, of 16 strong *IRAS* point sources associated with compact H II regions. The objectives were to determine the morphologies and physical properties of the ionized gas and to investigate the characteristics of their exciting stars. Our main results and conclusions are as follows.

1. The radio continuum brightness distribution was resolved for all the sources observed. Nine objects show simple morphologies: shell (three), cometary (three), core-halo (two), and bipolar (one), appearing to be excited by a single star. Seven objects exhibit complex radio continuum structure, which can be decomposed into multiple components.

2. The electron density and the diameter of compact and ultracompact H II regions follows a power-law relation of the form $N_e \propto D^{-1}$. This relation might be explained if the smallest regions of ionized gas correspond to the densest clumps within a larger inhomogeneous H II region excited by a single star.

3. The average infrared luminosity of the complex sources is 3 times higher than that of the simple sources. Their large IR luminosities and complex morphologies suggest that the complex sources are excited by multiple stars. Their IR and radio characteristics are best explained by models in which the excitation is due to a cluster of stars with spectral types earlier than B1, suggesting that the process of formation of luminous stars produces only massive stars. Probably as many as 50% of the *IRAS* point sources associated with unresolved (by single-dish antennas) radio continuum sources might be excited by a cluster of young O and B stars.

4. The 12 μm/25 μm and 12 μm/20 cm flux density ratios are remarkably similar for all objects in our sample. This suggests that the physical conditions of the dust are similar from source to source. The ratios are well explained by assuming a model in which the H II region is immediately surrounded by an optically thin region of warm dust that is in turn embedded in a large cloud of cool dust, $T_D \sim 26$ K, that is moderately thick at 12 μm. For an optical depth at 12 μm of the cool cloud between 1 and 3, we find that the temperature of the warm dust region is ~150 K and that its 12 μm opacity is ~0.003.

5. Assuming that the simple sources are excited by a single star, we conclude that typically ~55% of the ionizing stellar photons are absorbed by dust within the H II region. The infrared excesses of these sources are between 6 and 21, which can be fully accounted for by the radiation from the central star. Direct heating of dust by photons longward of the Lyman continuum limit accounts for ~60% of the total IR luminosity, ~15% is due to heating by Lyα photons, and ~25% is from radiation reemitted by the hot dust within the H II region.

We are grateful to our anonymous referee for a careful reading of the manuscript and for several helpful comments and suggestions. G. G. acknowledges support from the Henri Chrétien Award and from the Smithsonian Institution of Washington through a Short Term Visitor appointment at the Harvard-Smithsonian Center for Astrophysics.

REFERENCES

Antonopoulou, E., & Pottasch, S. R. 1987, A&A, 173, 108
Berulis, I. I., & Sorochenko, R. L. 1973, Soviet Astron., 17, 179
Brand, J. 1986, Ph.D. thesis, Univ. Leiden
Chini, R., Kreysa, E., Mezger, P. G., & Gemünd, H. P. 1986a, A&A, 154, L8
———. 1986b, A&A, 157, L1
Chini, R., Krügel, E., & Wargau, W. 1987, A&AS, 181, 378

Churchwell, E., Walmsley, C. M., & Cesaroni, R. 1990a, A&AS, 83, 119
Churchwell, E., Wolfire, M. G., & Wood, D. O. S. 1990b, ApJ, 354, 247
Cox, P., & Mezger, P. G. 1989, Astron. Astrophys. Rev., 1, 49
Downes, D., Goss, W. M., Schwarz, U. J., & Wouterloot, J. G. A. 1979, A&AS, 35, 1
Downes, D., Wilson, T. L., Bieging, J., & Wink, J. 1980, A&AS, 40, 379
Fazio, G. G. 1976, in Frontiers of Astrophysics, ed. E. H. Avrett (Cambridge: Harvard Univ. Press), 203
Felli, M., & Harten, R. H. 1981, A&A, 100, 42
Garay, G., & Rodríguez, L. F. 1990, ApJ, 362, 191
Gaume, R. A., & Mutel, R. L. 1987, ApJS, 65, 193
Goss, W. M., Lockhart, I. A., Fomalont, E. B., & Hardebeck, E. G. 1973, ApJ, 183, 843
Güsten, R., & Mezger, P. G. 1983, Vistas Astron., 26, 159
Habing, H. T., & Israel, F. P. 1979, ARA&A, 17, 345
Handa, T., Sofue, Y., Nakai, N., Hirabayashi, H., & Inoue, M. 1987, PASJ, 39, 709
Hardebeck, E. G., & Wilson, W. J. 1971, ApJ, 179, L123
Harris, S. 1976, MNRAS, 174, 1
Haschick, A. D., & Ho, P. T. P. 1983, ApJ, 267, 638
Herbig, G. H. 1982, in Symposium on the Orion Nebula to Honor Henry Draper, ed. A. E. Glassgold, P. J. Huggins, & E. L. Schucking, Ann. NY Acad. Sci., 395, 64
Hildebrand, R. H. 1983, QJRAS, 24, 267
Ho, P. T. P., & Haschick, A. D. 1981, ApJ, 248, 622
Keto, E., Ho, P. T. P., & Haschick, A. D. 1987, ApJ, 318, 712
Krassner, J., Pipher, J. L., Savidoff, M. P., & Soifer, B. T. 1983, AJ, 88, 972
Krishna Swamy, K. S., & O'Dell, C. R. 1968, ApJ, 151, L61
Kurtz, S., Churchwell, E., & Wood, D. O. S. 1993, in preparation
Matthews, H. E., Goss, W. M., Winnberg, A., & Habing, H. J. 1973, A&A, 29, 309
———. 1977, A&A, 61, 261
Mezger, P. G., & Henderson, A. P. 1967, ApJ, 147, 471
Miller, G. E., & Scalo, J. M. 1979, ApJS, 41, 513
Moran, J. M. 1983, Rev. Mexicana Astron. Af., 7, 95
Panagia, N. 1973, AJ, 78, 928
Panagia, N., & Walmsley, C. M. 1978, A&A, 70, 411
Petrosian, V., Silk, J., & Field, G. B. 1972, ApJ, 177, L69
Pottasch, S. R., et al. 1984, A&A, 138, 10
Shu, F. H., Adams, F. C., & Lizano, S. 1987, ARA&A, 25, 23
Van Buren, D., Mac Low, M., Wood, D. O. S., & Churchwell, E. 1990, ApJ, 353, 570
Wink, J. E., Altenhoff, W. J., & Mezger, P. G. 1982, A&A, 108, 227 (WAM)
Wood, D. O. S., & Churchwell, E. 1989, ApJS, 69, 831
Woodward, C. E., Helfer, H. L., & Pipher, J. L. 1985, A&A, 147, 84